Doctoral Dissertation (Censored)

博士論文 （要約）

The Olfactory Imprinting during the Critical Period in Mice.

（マウス嗅覚系の臨界期における刷り込み記憶形成機構の解明）

Nobuko Inoue

井上　展子

Contents

Abstract

Neural circuits are formed based on a genetic program and further refined by neuronal activity during the neonatal period. This dissertation shows that, in the mouse olfactory system, the glomerular map is not merely refined but newly connected to second-order neurons, by odorant-receptor-derived activity. I analyzed a ligand molecule, Semaophorin 7A (Sema7A), expressed in olfactory sensory neurons (OSNs) in an activity-dependent manner, and its receptor, Plexin C1 (PlxnC1), localized to dendrites of mitral/tufted (M/T) cells in the first week after birth. In Sema7A or PlxnC1 knockout (KO) mice, initiation of synapse formation and M/T-cell dendrite selection were perturbed. In vitro reconstitution and in vivo rescue experiments demonstrated that Sema7A-PlxnC1 interaction is essential to form the post-synaptic assembly. These results showed that Sema7A signaling is key to inducing activity-dependent post-synapse events and dendrite selection in M/T-cells during the neonatal period. Then, what is the meaning for activity-dependency of synapse formation? Interestingly, odor exposure in neonates increases Sema7A expression in the responding glomeruli recruiting primary dendrites of mitral/tufted cells. This enhancement not only increases the sensitivity to the conditioned odor but also reduces stress reactions by lowering adrenocorticotropic hormone (ACTH). These imprinting effects were observed even when the odor quality is innately aversive. However, imprinting does not occur when odor conditioning is performed later than the first week after birth or in the absence of Sema7A/PlxnC1 signaling. I showed that the imprinted odor activates the anterior medial-amygdala that mediates attractive social responses, and suppresses the amygdalo-piriform transition area known to induce ACTH. Lack of Sema7A/PlxnC1 signaling in neonates does not induce imprinting, causing impairment of odor-mediated social behaviors as adults. Knockout and rescue experiments indicate that peptide hormone, oxytocin, in neonates may be involved in integrating positive qualities into the imprinted odor memory. These results give us understanding of the molecular mechanism for olfactory imprinting by sensory inputs during the neonatal critical period.

Introduction

Mammalian sensory systems are generated by a combination of activity-independent and -dependent processes. The basic architecture of sensory systems is built based on a genetic program[1, 2, 3]. However, the neural circuits are further refined in an activity-dependent manner[4, 5, 6, 7, 8]. In neonates, there is a narrow time frame, referred to as the critical period that allows proper development in response to environmental cues. This activity-dependent process is initially plastic for limited time frame then becomes irreversible. If the circuit is left unstimulated, the brain development served by that circuit is impaired. Thus, sensory inputs during the neonatal period are important to make the functional system.

Unlike other sensory systems, olfactory sensory neurons (OSNs) in mice are constantly renewed throughout the animal's life[9, 10, 11]. Although OSNs are replaced and form new connections with second-order neurons, mitral/tufted cells (M/T cells), proper circuits cannot be regenerated once the existing OSNs are completely ablated after the early neonatal period. This period of olfactory circuit formation has been referred to as the critical period[12, 13]. However, the olfactory critical period has not been precisely defined at the molecular level, and the key process that makes this time-window critical has yet to be understood.

The mouse olfactory system detects a variety of odorants using a repertoire of approximately 1,000 ~ odorant receptors (ORs)[14]. Each olfactory sensory neuron expresses one functional OR gene[15], and OSN axons expressing the same OR species converge to a specific set of glomeruli in the olfactory bulb (OB)[16]. Since an odorant activates multiple OR species[17], odor signals detected in the olfactory epithelium (OE) are converted to a unique combination of activated glomeruli, enabling the mammalian brain to discriminate various odorants[18]. The odor information is further processed by local circuits in the OB and conveyed by M/T cells for decision making to various areas in the olfactory cortex (OC)[6] (Introduction).

During embryonic development, a coarse olfactory map is generated by a combination of anatomical locations of OSNs, and the OR-derived cAMP signals[19, 20]. After OSN axons reach their approximate destinations in the OB, refinement of an olfactory map occurs through fasciculation of OSN axons in an activity-dependent manner[21]. Although most of these processes take place by axon-axon interactions of OSNs[22], proper connections are needed between OSN axons and the M/T-cell dendrites. In contrast to the primary projection of OSN axons, little is known about synapse

formation with M/T-cell dendrites. For example, what molecule mediates the synapse formation between OSN axons and M/T-cell dendrites? How do they decide their partners for proper synapse formation? At first, I searched for a pair of ligand and receptor molecules that are involved in synapse formation and dendrite selection of M/T cells.

Furthermore, odor information is roughly sorted into distinct functional domains in the olfactory bulb (OB) during the process of primary projection of OSNs[23, 24]. Odor information is then conveyed by M/T cells to various areas in the OC to induce responses. It has been reported that attractive social information is transmitted to a part of medial amygdala (MeA) [25, 26, 27], whereas aversive/fear information is conveyed to a part of the cortical amygdala (CoA) [28, 29, 30]. These hard-wired circuits connecting the OB and OC regions are thought to be genetically programmed[25, 29, 30], however, their outputs can be modulated by neonatal experiences. In mammals, neonatal environmental odor exposure can affect odor perception and behavior as adults[31, 32, 33, 34]. Salmon and trout are known to return to their mother river based on olfactory memory[35]. In the visual system, ducklings follow the first moving object upon hatching recognizing it as the parents[36, 37]. Although such phenomena are widely known, little is understood about how imprinting is established and how the imprinted memory modulates innate behavioral decisions. In conjunction with the above, I studied the olfactory imprinting in mice by analyzing activity-dependent synapse formation at molecular level.

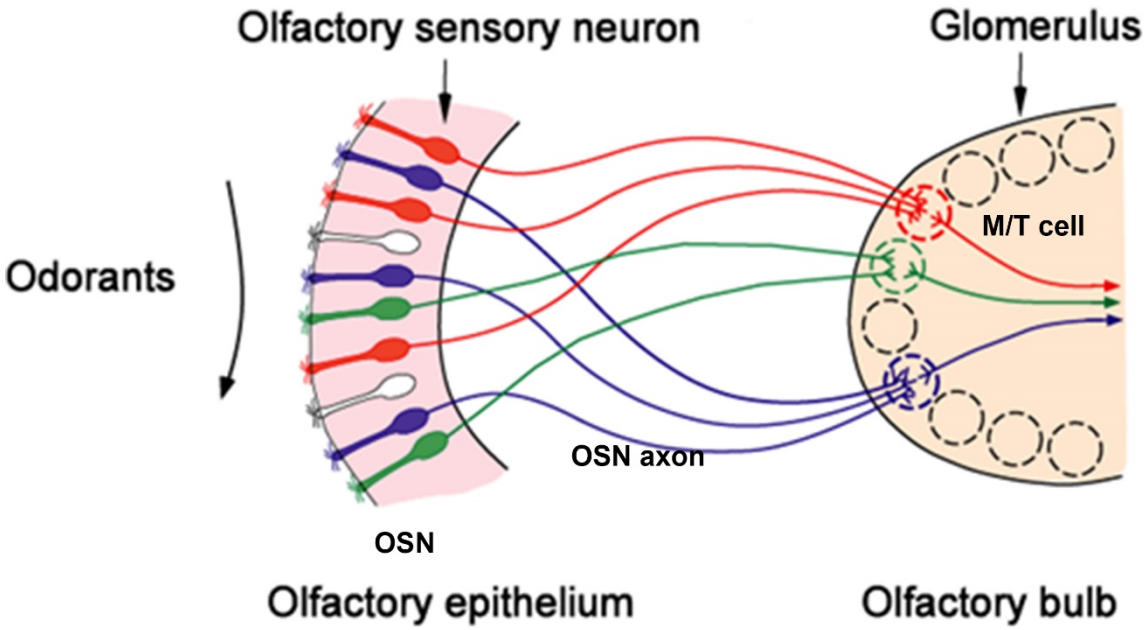

Introduction Schematic diagram of the mouse olfactory system.

Chapter 1 Sema7A expression in OSN axons

At first, I searched for a receptor and ligand pair each of which was expressed by OSN axons or M/T-cell dendrites for initiating the synapse formation in glomeruli. I examined 26 different genes of axon guidance, cell adhesion, and signaling molecules for their expression in the OE and OB by in situ hybridization and immunostaining (Table 1). Among them, Semaphorin 7A (Sema7A) and its candidate receptor, Plexin C1 (PlxnC1), were found to be expressed in OSNs and M/T-cell dendrites, respectively during the neonatal period. Immunostaining of OB sections revealed that Sema7A was localized to the axon termini of OSNs in a mosaic pattern (Fig. 1a). Immuno-electronmicroscopy demonstrated that Sema7A is localized to the pre-synaptic terminal of OSN axons (Fig. 1b). Levels of Sema7A expression are determined by OR species, e.g., high in rI7, medium in MOR29B, and low in MOR29A glomeruli (Fig. 1c). This observation indicates that Sema7A expression is downstream of the OR activity as known for glomerular segregation molecules, e.g., Kirrel2 and Kirrel3[22]. When one naris was occluded at postnatal day 0-6 (P0-6), Sema7A expression in the OE was reduced on the occluded side (Fig. 1d left), showing that Sema7A expression is regulated by OSN neuronal activity. Activity dependency of Sema7A expression was confirmed by the analysis of CNG-A2-defficient mice, a component of the cyclic nucleotide-gated (CNG) channel[38]. Since the *CNG-A2* gene is on the X chromosome, mosaicism can occur among OSNs for CNG-A2 activity due to stochastic X-chromosome inactivation in the female[39]. In the CNG-A2$^{+/-}$ female mice, duplicated glomeruli are formed: one is for CNG-A2^{+} axons and the other for CNG-A2^{-}. In rI7 glomeruli, where Sema7A levels are high, at P5, Sema7A levels in the CNG-A2^{-} glomerulus were much lower than in that of CNG-A2^{+} (Fig. 1d middle). We also analyzed the mutant rI7 (RDY) defective in G-protein coupling[21]. In OSNs where rI7 (RDY) was expressed, Sema7A expression was not produced (Fig. 1d right), because cAMP for opening CNG-A2 channels is not generated by the mutant rI7. These results show that Sema7A expression is regulated by OR-derived neuronal activity in OSNs.

Expression of axon guidance, signaling, and adhesion molecules in the OE and OB

gene	name	function	OE (mRNA)	OB (mRNA)	M/T dendrites (protein)
ephA5	Ephrin type-A receptor 5	protein-tyrosine kinase	+	-	-
efna5	ephrin-A5	ligand of Eph-related Kinase	+	+	-
s100A5	S100 calcium binding protein A5	calcium binding	+	-	-
kirrel2	kin of IRRE like 2	cell adhesion	+	-	-
kirrel3	kin of IRRE like 3	cell adhesion	+	+	-
pcp4	Purkinje cell protein 4	calmodulin binding	+	-	-
ptprn	protein tyrosine phosphatase type-N receptor	signal transduction	+	+	-
ptprf	protein tyrosine phosphatase type-F receptor	signal transduction	+	-	-
nrp1	neuropilin 1	signal transduction	+	+	-
nrp2	neuropilin 2	signal transduction	+	+	-
nph3	neurexophilin 3	neuropeptide	+	-	-
sema3a	semaphorin 3a	axon guidance	+	+	-
sema3f	semaphorin 3f	axon guidance	+	-	-
sema4d	semaphorin 4d	axon guidance	-	+	-
sema7a	semaphorin 7a	axon guidance	+	+	-
plxna1	plexin a1	signal transduction	+	-	-
plxna2	plexin a2	signal transduction	-	-	-
plxna3	plexin a3	signal transduction	+	+	-
plxna4	plexin a4	signal transduction	-	-	-
plxnb1	plexin b1	signal transduction	+	-	-
plxnb2	plexin b2	signal transduction	+	-	-
plxnb3	plexin b3	signal transduction	+	-	-
plxnc1	plexin c1	signal transduction	-	+	+
itgb1	integrin beta 1	cell adhesion	-	-	-
omp	olfactory marker protein	signal transduction	+	-	-
pcdh21	protocadherin-21	cell adhesion	-	+	+

OE and OB sections at P4 were analyzed by *in situ* hybridizaion, OB sections were analyzed by immunohistchemistry. **+**, detected; **-**, not detected

Table 1 Expression of axon guidance, signaling and adhesion molecules in the OE and OB.

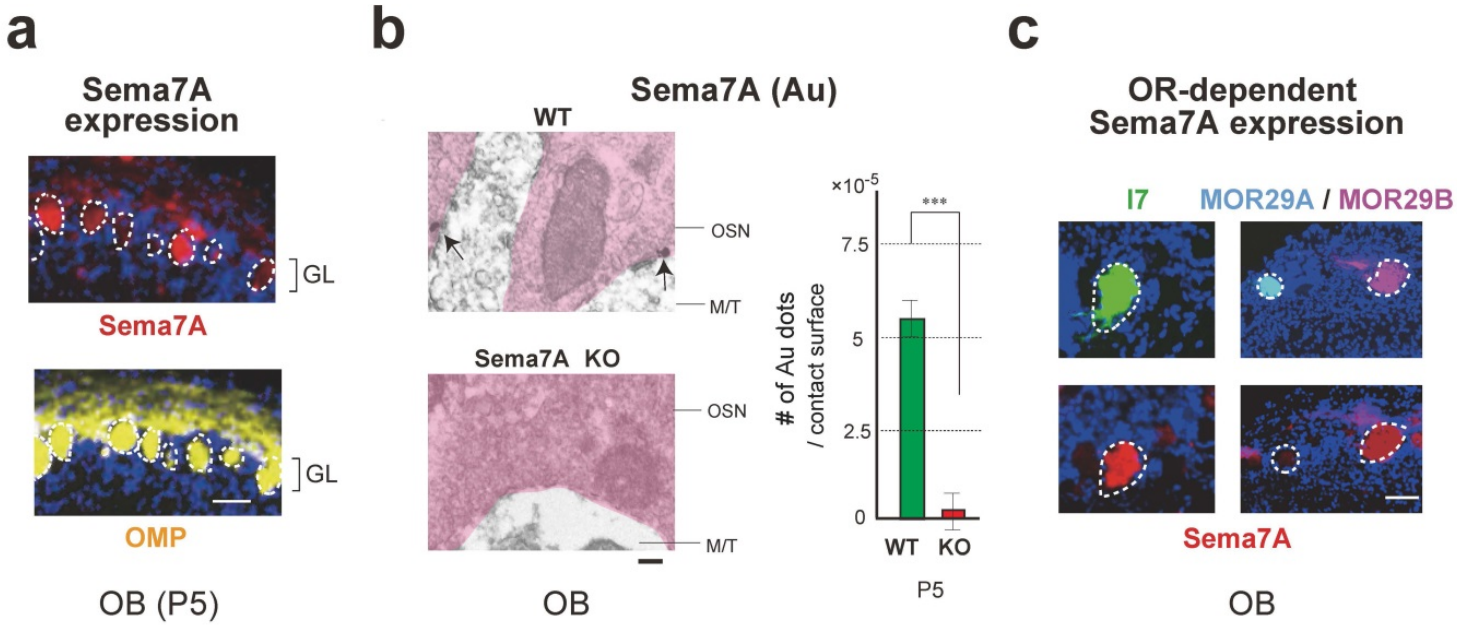
a
Sema7A expression
GL
Sema7A
GL
OMP
OB (P5)
b
Sema7A (Au)
WT
OSN
M/T
Sema7A KO
OSN
M/T
OB
×10-5
7.5
5
2.5
0
***
# of Au dots / contact surface
WT KO
P5
c
OR-dependent Sema7A expression
I7
MOR29A / MOR29B
Sema7A
OB

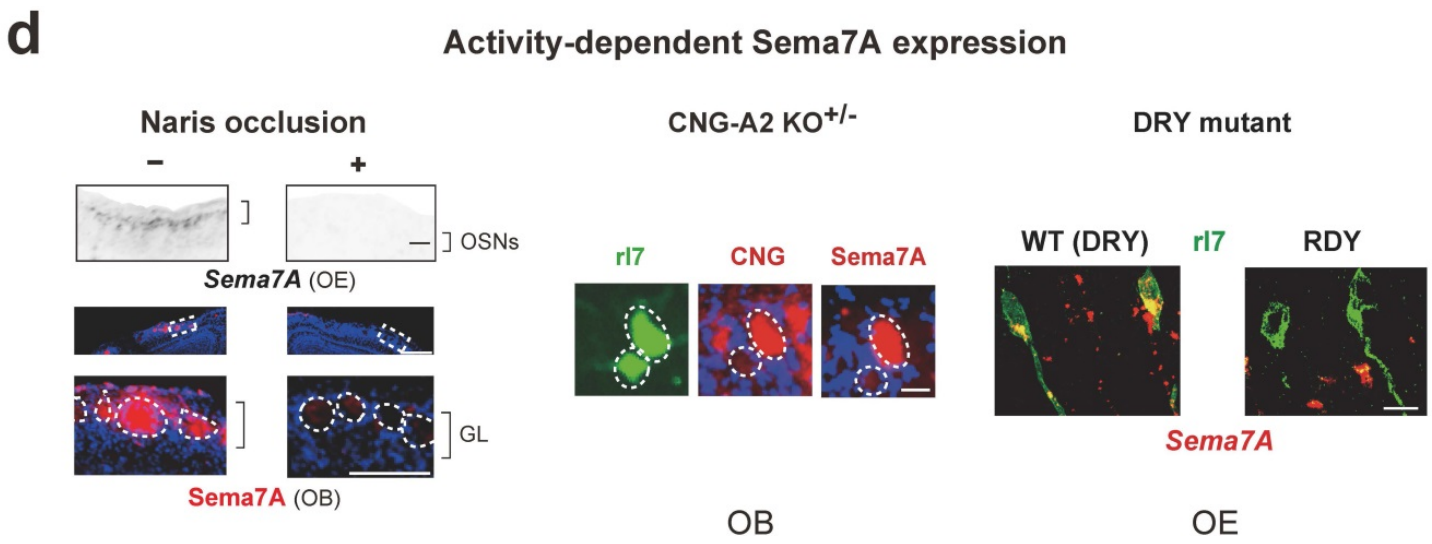
d
Activity-dependent Sema7A expression
Naris occlusion
–
+
OSNs
Sema7A (OE)
GL
Sema7A (OB)
CNG-A2 KO+/-
rI7
CNG
Sema7A
OB
DRY mutant
WT (DRY)
rI7
RDY
Sema7A
OE

Fig. 1 OR-derived activity-dependent Sema7A expression in OSN axons.

a, Distribution of Sema7A in the GL of the OB. OB sections of the WT at P5 were immunostained with antibodies against Sema7A and OMP. Scale bar, 25 μm. **b**, Detection of Sema7A in the OSN axon termini. Immuno-electronmicroscopy identified Au-labeled Sema7A (arrows) in the pre-synaptic axon termini of OSNs at P5. Au signals were not detected in the Sema7A KO. The number of signals a contact surface was counted (right). ***$p<0.005$ (Student's *t*-test). Error bars indicate SD. n=3 animals for each. Scale bar, 300 nm. **c**, Variable Sema7A expression among different glomeruli. OB sections at P10 were immunostained with antibodies against Sema7A. EYFP-tagged rI7, ECFP-tagged MOR29A and EYFP-tagged MOR29B glomeruli were detected by immunofluorescence staining with anti-GFP antibodies. Scale bar, 25 μm. **d**, Sema7A expression in an activity-dependent manner. Left, Down-regulation of Sema7A expression by naris occlusion. Mice were unilaterally naris-occluded at P0. OE sections at P6 were analyzed by *in situ* hybridization. OB sections at P6 were analyzed by immunostaining with anti-Sema7A antibodies. (+) occluded, (-) unoccluded. Scale bars, 50 (upper), 100 (lower) μm. Middle, Sema7A expression regulated by CNG-channel-dependent activity. Duplicated glomeruli of rI7 in the CNG-$A2^{+/-}$ KO were analyzed for Sema7A expression at P5. EYFP-tagged rI7 glomeruli were detected by immunofluorescence staining with anti-GFP antibodies. OB sections were immunostained with anti-CNG-A2 and Sema7A antibodies. Scale bar, 25 μm. Right, Sema7A expression regulated by OR-derived activity. In a DRY-motif mutant of rI7 *Sema7A* expression is suppressed because it does not generate cAMP. OE sections expressing the WT and DRY-motif mutant (RDY) rI7 were analyzed by *in situ* hybridization for *Sema7A* expression at P5. OSNs expressing the EYFP-tagged rI7 were detected by immunofluorescence staining with anti-GFP antibodies. Scale bar, 10 μm. GL, glomerular layer.

Chapter 2 PlxnC1 expression in M/T-cell dendrites

Next I studied the candidate receptors for Sema7A in M/T cells. Both in the immune and in the central nervous systems, PlxnC1 and Integrin β1 are known as receptors for Sema7A[40-42]. At early developmental stages, *PlxnC1*, not *Integrin β1*, is transcribed in M/T cells by *in situ* hybridization (Table 1 and Fig. 2a). PlxnC1 protein is detected to M/T-cell dendrites (Fig. 2b). Staining of PlxnC1 is weak in glomeruli in the neonates, becomes stronger at P3-P5, and gradually disappears after P8. PlxnC1 is detected evenly in all glomeruli at P3-5 regardless of OR species. In the adult, both PlxnC1 and Integrin β1 are produced in M/T cells, but neither of them is detected in M/T-cell dendrites within glomeruli (Fig. 2b). I examined whether Sema7A in OSN axons indeed interacts with PlxnC1 in M/T cells in the glomeruli by alkaline phosphatase (AP) staining[22, 43]. I made both PlxnC1 and Sema7A fused to AP as affinity probes. Serial OB sections were treated with AP-fusion proteins and also immunostained with antibodies against Sema7A or PlxnC1. Staining for AP-fusion proteins of PlxnC1 and Sema7A showed similar glomerular patterns as anti-Sema7A and anti-PlxnC1 antibodies did, respectively (Fig. 3). Each KO was analyzed as a negative control. These results indicate that PlxnC1 serves as a receptor for Sema7A, interacting with each other between OSN axons and M/T-cell dendrites.

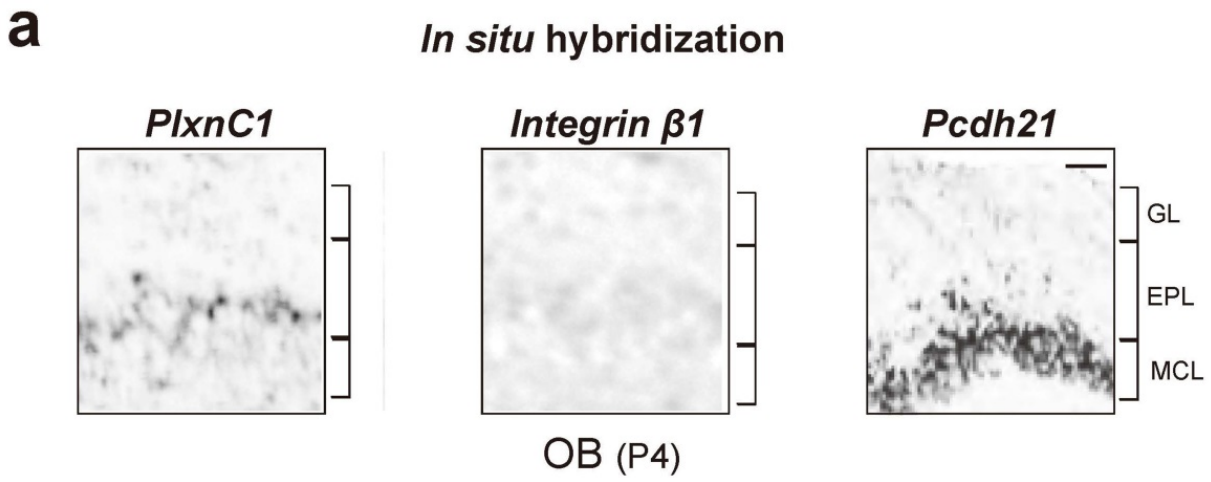
a
In situ hybridization
PlxnC1
Integrin β1
Pcdh21
GL
EPL
MCL
OB (P4)

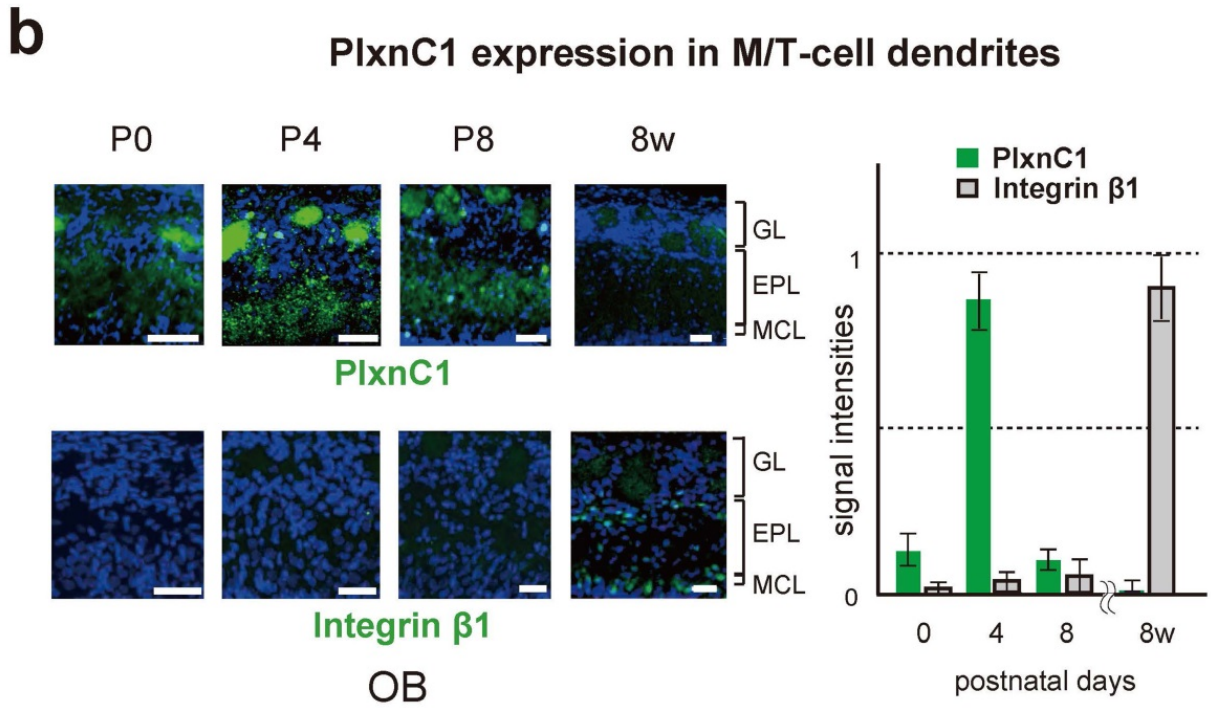
b
PlxnC1 expression in M/T-cell dendrites
P0
P4
P8
8w
GL
EPL
MCL
PlxnC1
Integrin β1
OB
PlxnC1
Integrin β1
signal intensities
1
0
0
4
8
8w
postnatal days

Fig. 2 PlxnC1 localized to the M/T-cell dendrites in neonates.

a, Gene expression of candidate receptors for Sema7A in the OB. OB sections at P4 were analyzed by *in situ* hybridization with the probes for *PlxnC1*, *Integrinβ1*, and *Pcdh21* (M/T-cell marker). n=6 animals. Scale bar, 30 μm. **b**, Temporal regulation of PlxnC1 localization in the OB. OB sections were immunostained with anti-PlxnC1 and Integrinβ1 antibodies at various developmental stages. Relative signal intensities (GL/EPL) are compared at different day points. n=2 animals except for P4 (n=6). Scale bars, 30 μm. GL, glomerular layer; EPL, external plexiform layer; and MCL, mitral cell layer.β

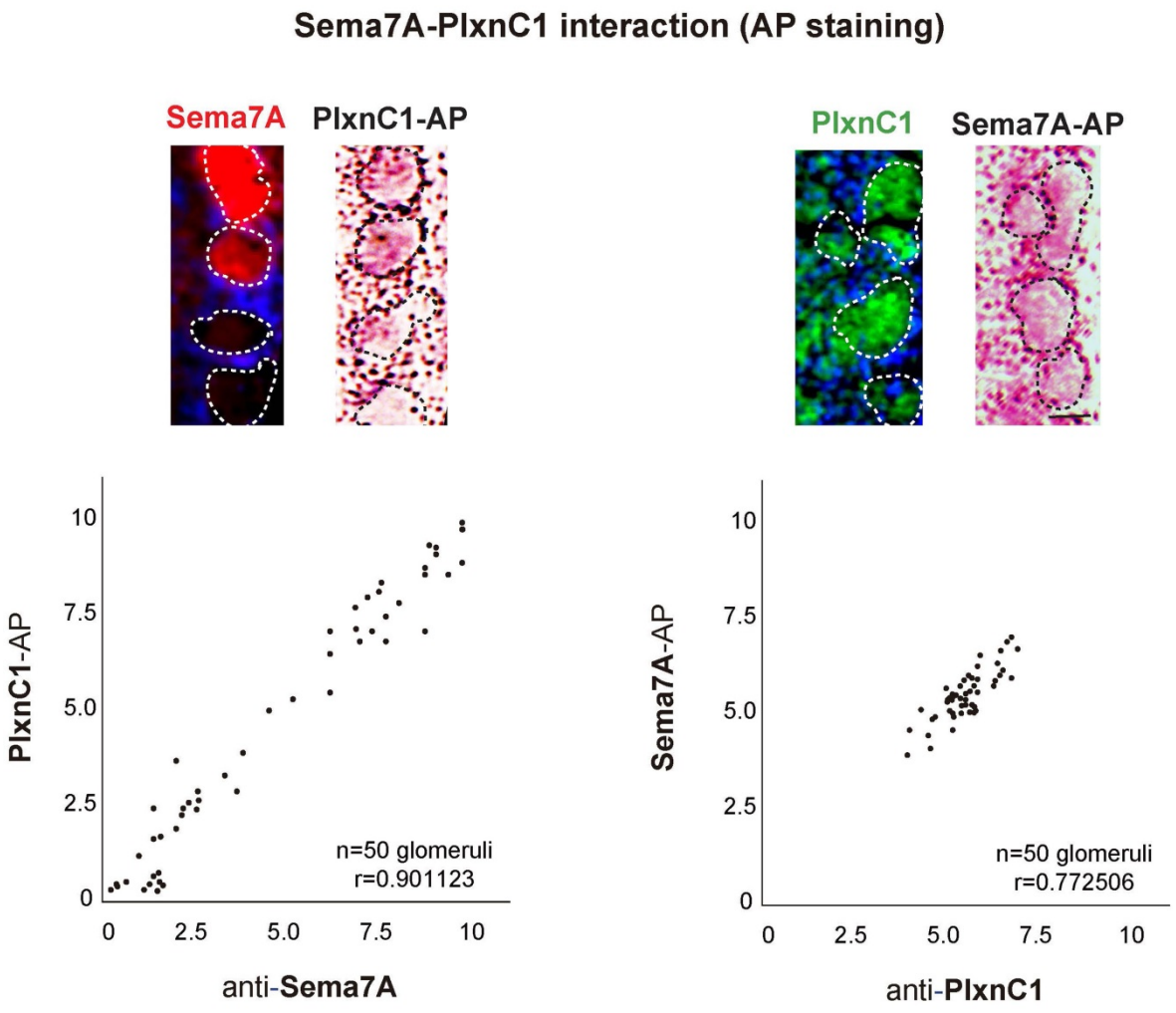

Fig. 3 *In vivo* interaction of Sema7A and PlxnC1 in the OB.

The binding assay with AP-fusion proteins detected Sema7A-PlxnC1 interaction in the OB. Consecutive OB sections at P4 were stained with PlxnC1-AP and immunostained with antibodies against Sema7A (left) and also with Sema7A-AP and immunostained with antibodies against PlxnC1 (right). Positive correlations are read out between the AP-staining and immunostaining signals. The Pearson's correlation coefficient was shown (r). n=50 glomeruli. Scale bar, 25 μm.

Chapter 3 KO analysis of Sema7A/PlxnC1 signaling

To elucidate the *in vivo* function of Sema7A/PlxnC1 signaling, at first, I analyzed the glomerular map formation of the Sema7A KO[41] after crossing with Tg MOR29B[44] or MOR28 knock-in mice[45], because other semaphorin molecules are known to affect OSN projection to the OB[20, 21]. Whole mount view of the OB from the Sema7A KO at P8 did not reveal any notable defects in OSN projection or fasciculation in glomeruli (Fig. 4 and Table 2). However, synapse formation appeared to be perturbed in the Sema7A KO. Immunostaining of rI7 glomeruli with synaptic markers, vGlut2 and GluR1[46-48], revealed that synapse formation was impaired in the Sema7A KO at P5 (Fig. 5a). Synapse formation remained defective in the Sema7A KO into adulthood (Fig. 5a). Furthermore, dendrite maturation of M/T cells was also defected. I studied M/T-cell dendrite selection for the rI7 glomeruli in the Sema7A KO. To visualize dendrites[49], Lucifer yellow (LY) was injected from the rI7 glomeruli into one connecting M/T cell (Fig. 6). I counted the numbers of M/T cells with primary dendrite as mature and with multiple dendrites to the glomerular layer (GL) as immature. In the Sema7A KO, dendrite selection of M/T cells was perturbed, although dendrite extension was normal (Fig. 5b). I also analyzed about PlxnC1. The M/T-cell-specific PlxnC1 conditional KO (PlxnC1 cKO) was generated using the Pcdh21-Cre mouse[50] as a driver. It was confirmed that PlxnC1 was absent in the KO by immunostaining, although the mitral cell layer (MCL) was seen to be normally formed (Fig. 7). It means that migration to the OB of M/T cells occurred normally. I then studied synapse formation and dendrite selection of M/T cells. In the cKO, M/T-cell dendrite extension took place. But, synapse formation was impaired (Fig. 5c) and dendrite selection was delayed (Fig. 5d) as seen in the Sema7A KO. Synaptic structures were studied in detail by electron microscopy (EM) in these KOs (Fig. 8a and b). It was confirmed that initiation of synapse formation and post synaptic density (PSD) were not seen, although membrane attachment was taking place. These results suggest that Sema7A/PlxnC1 interaction is needed for synapse formation and dendrite selection of M/T cells. It is interesting that in the Sema7A^{high}-type glomeruli (e.g., for MOR29B), synapse formation and dendrite selection occur a few days earlier than in the Sema7A^{low}-type (e.g., for MOR29A) (Fig. 9), although these two OR have very similar DNA, amino acid sequence and OSN projection pattern/timing[44]. These observations indicate that Sema7A expression promotes synapse formation and dendrite selection of M/T cells in newborn.

Glomerular formation and localization in the OB

MOR29B glomeruli	WT at P6 (n=8)	Sema7A KO at P6 (n=8)	Nrp1 OSN-specific KO at P6 (n=4)
Dorsal view (OB size) (mm^2)	0.1325 ± 0.010	0.1325± 0.0095 (n.s.)	0.1281 ± 0.007 (n.s.)
1. Radial position of medial glomeruli (in degrees where 90° is the ventral midline)	75.94 ± 2.33	78.40 ± 1.55 (n.s.)	ec 65.71 ± 4.890 **
2. Distance of medial glomeruli from the caudal end of the OB (μm)	201.25 ± 13.94	197.5±14.40 (n.s.)	ec 345.71 ± 46.50 **
3. The number of ectopic glomeruli	0.5 ± 0.15	0.5 ± 0.12 (n.s.)	2.1 ± 0.34 **
MOR28 glomeruli	WT at P8 (n=5)	Sema7A KO at P8 (n=6)	Sema3F OSN-specific KO at P8 (n=4)
Ventral view (OB size) (mm^2)	0.17 ± 0.0209	0.172 ± 0.0146 (n.s.)	0.165 ± 0.008 (n.s.)
1. Radial position of medial glomeruli (in degrees where 90° is the ventral midline)	76.4 ± 3.611	76.2 ± 3.429 (n.s.)	ec 43.42 ± 3.579 **
2. Distance of medial glomeruli from the caudal end of the OB (μm)	145.4 ± 28.72	146.8 ± 29.60 (n.s.)	ec 174.57 ± 16.69 **
3. The number of ectopic glomeruli	0.4 ± 0.48	0.4 ± 0.5 (n.s.)	2.2 ± 0.45 **

means ± SE. **p<0.01; n.s.:no significant difference was found.

EYFP-tagged MOR29B glomeruli at P6 and MOR28 at P8 were analyzed in the WT, Sema7A KO, OSN-specific Nrp1 KO, and OSN-specific Sema3F KO. The OB size (mm^2), radial position (degree) and distance from the end of OB (μm) were measured. **p<0.01 (Students t test). No significant difference in glomerular formation was found between the WT and Sema7A KO. A schematic diagram for the glomerular measurements is shown. ec, ectopic glomeruli.

Table 2 Glomerular formation and localization in the OB of the Sema7A KO.

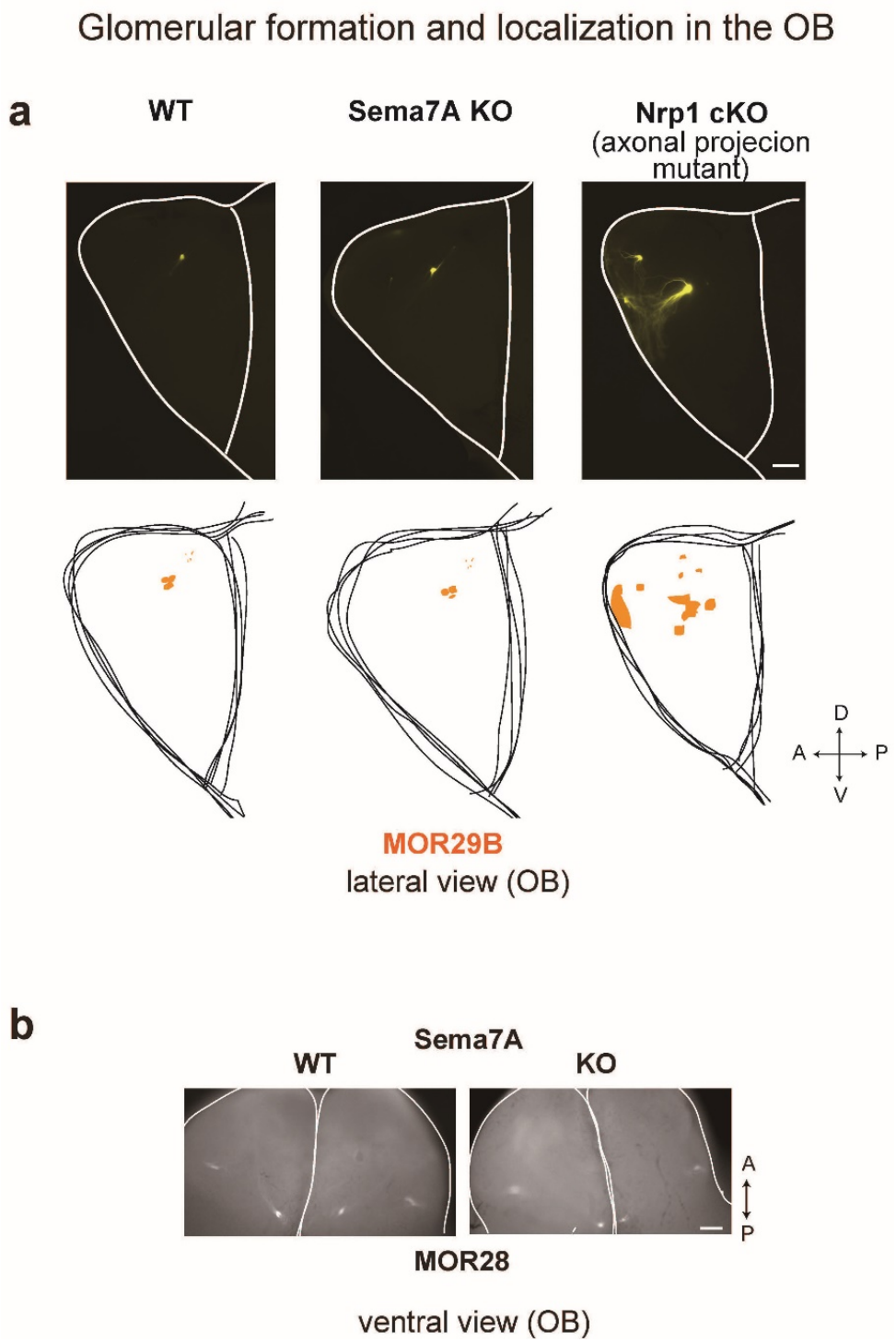
Glomerular formation and localization in the OB
a
WT
Sema7A KO
Nrp1 cKO
(axonal projecion
mutant)
D
A
P
V
MOR29B
lateral view (OB)
b
Sema7A
WT
KO
A
P
MOR28
ventral view (OB)

Fig. 4 Axonal projection of OSNs in the Sema7A KO.

a, The tg *MOR29B* gene was tagged with *EYFP* for immunofluorescence staining of the MOR29B glomeruli in the OB. Lateral views are shown. Tg animals were crossed with Sema7A total KO or OSN-specific cKO of Nrp1(OSN axonal project molecule[21]) and analyzed at P20. Locations of the MOR29B glomeruli are schematically shown. n=4 for each mouse strain. Scale bar, 50 μm. **b**, The *MOR28* gene was tagged with *EGFP* for immunofluorescence staining of the MOR28 glomeruli in the OB. The MOR28 knock-in mice were mated with Sema7A total KO. Ventral views are shown. The WT and Sema7A KO were analyzed at P10. n=5 for each mouse strain. Scale bar, 50 μm. D, dorsal; V, ventral; A, anterior; and P, posterior.

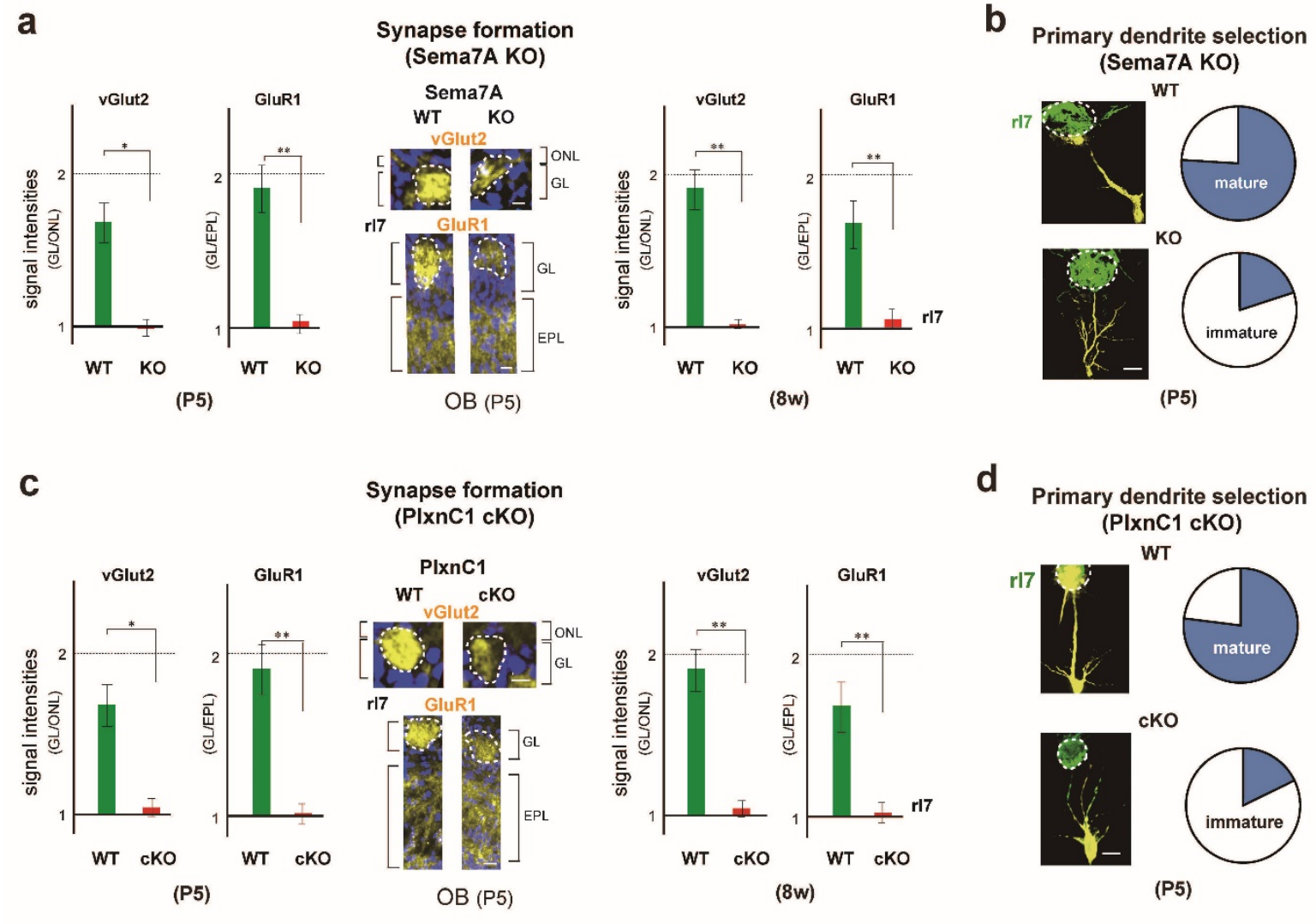
a
Synapse formation
(Sema7A KO)
vGlut2
GluR1
signal intensities
(GL/ONL)
(GL/EPL)
WT
KO
(P5)
Sema7A
WT
KO
vGlut2
ONL
GL
rl7
GluR1
GL
EPL
OB (P5)
(8w)
b
Primary dendrite selection
(Sema7A KO)
WT
KO
rl7
mature
immature
(P5)
c
Synapse formation
(PlxnC1 cKO)
PlxnC1
cKO
d
Primary dendrite selection
(PlxnC1 cKO)

Fig. 5 Synapse formation and dendrite maturation in the KOs of Sema7A and PlxnC1.

a, Synapse formation within glomeruli in the Sema7A KO. OB sections of the WT and Sema7A KO at P5 and 8w were immunostained with anti-vGlut2 and GluR1 antibodies respectively. Staining mages for rI7 glomeruli are shown for P5 sections. Signal intensities within the rI7 glomeruli were normalized by signals in the ONL for pre-synaptic signals and in the EPL for post-synaptic signals. Fluorescent signals of GL/ONL and GL/EPL in glomeruli are compared between the WT and KO. Scale bars, 25 μm. *p<0.05, **p<0.01 (Student's *t*-test). Error bars indicate SD (n=5, 6, 2, 3 animals). **b**, Dendrite maturation of M/T cells in the Sema7A KO. EYFP-tagged rI7 glomeruli (green) were immune-stained with anti-GFP antibodies. M/T cells (yellow) were visualized by LY injection into the rI7 glomeruli of the WT and Sema7A KO at P5 (left). The numbers of M/T cells with one dendrite (mature) and those with multiple dendrites (immature) to glomerular layer were counted for the rI7 glomeruli. The ratios (%) of mature (blue) and immature (white) M/T cells are shown (right): WT, 26/34 (76.5 %); KO, 8/34 cells (23.5 %). n= 20 glomeruli. Scale bar, 10μm. **c**, Synapse formation within glomeruli in the PlxnC1 cKO. OB sections of the WT and PlxnC1 cKO at P5 and 8w were analyzed by immunostaining for synapse markers. Staining photos are for P5 sections. Signal intensities within the rI7 glomeruli were shown as the Sema7A KO. Scale bars, 25 μm. *p<0.05, **p<0.01 (Student's *t*-test). Error bars indicate SD (n=5, 5, 2, 3 animals). **d**, Dendrite maturation in the PlxnC1 cKO. M/T cells (yellow) were visualized by LY injection into the rI7 glomeruli of the WT and cKO at P5 (left). The ratios (%) of mature (blue) and immature (white) M/T cells are shown (right): WT, 24/31 (77.4 %); KO, 7/31 (22.6 %). n= 23 glomeruli. Scale bar, 20 μm.

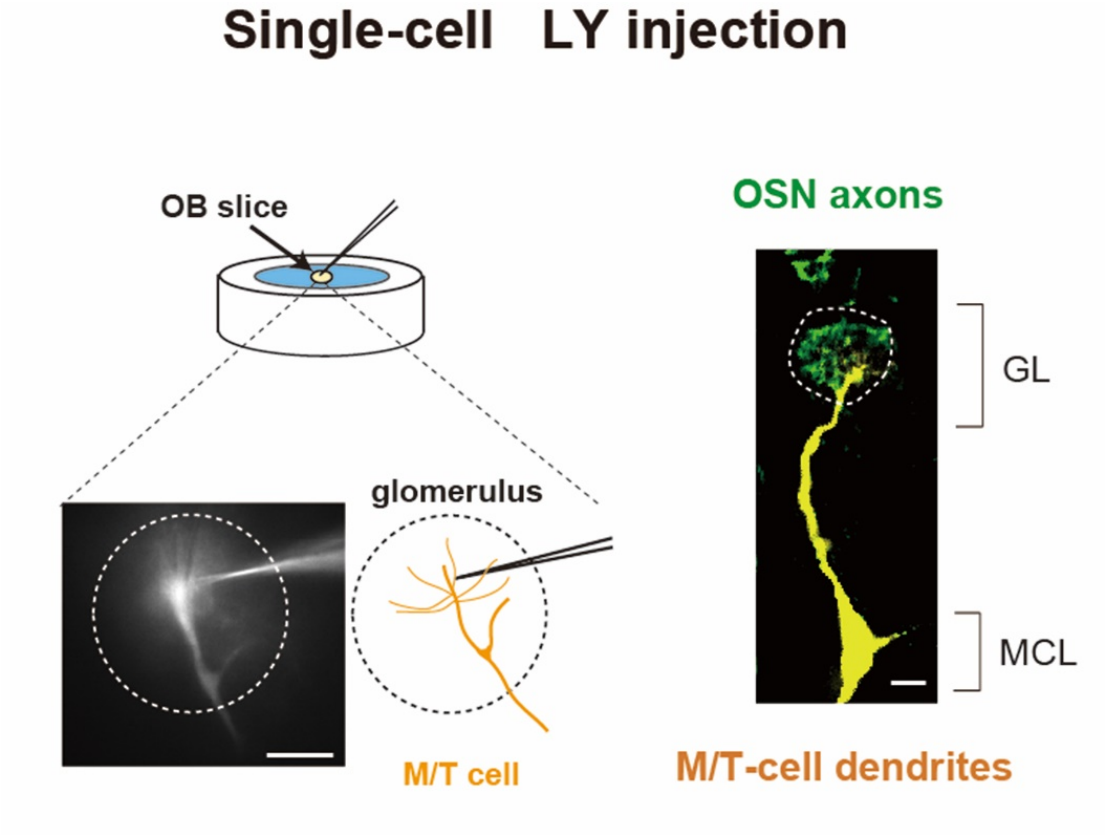

Fig. 6 Single cell labelling by LY injection.

M/T cells were visualized by Lucifer yellow (LY) injection into an OB slice containing GFP-labeled glomerulus. For example, one mature mitral cell are shown with the MOR29A^{+} OSN stained green for ECFP. Scale bar, 10 μm. GL, glomerular layer; MCL, mitral cell layer.

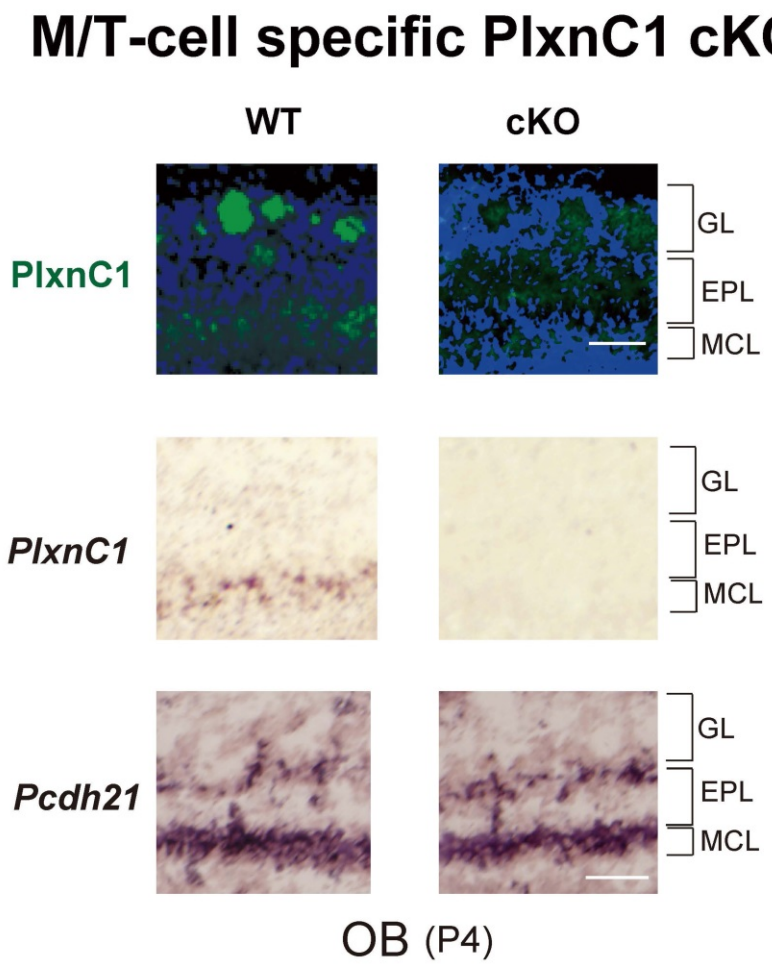

Fig. 7 M/T cell-specific KO for PlxnC1.

Loss of PlxnCl expression in the cKO. OB sections at P4 were immunostained with anti-PlxnC1 antibodies for both the WT and cKO. Transcription of the *PlxnC1* gene was also analyzed by *in situ* hybridization. *Pcdh21*, M/T-cell marker, in both the WT and cKO. Scale bars, 50 μm. GL, glomerular layer; EPL, external plexiform layer; and MCL, mitral cell layer.

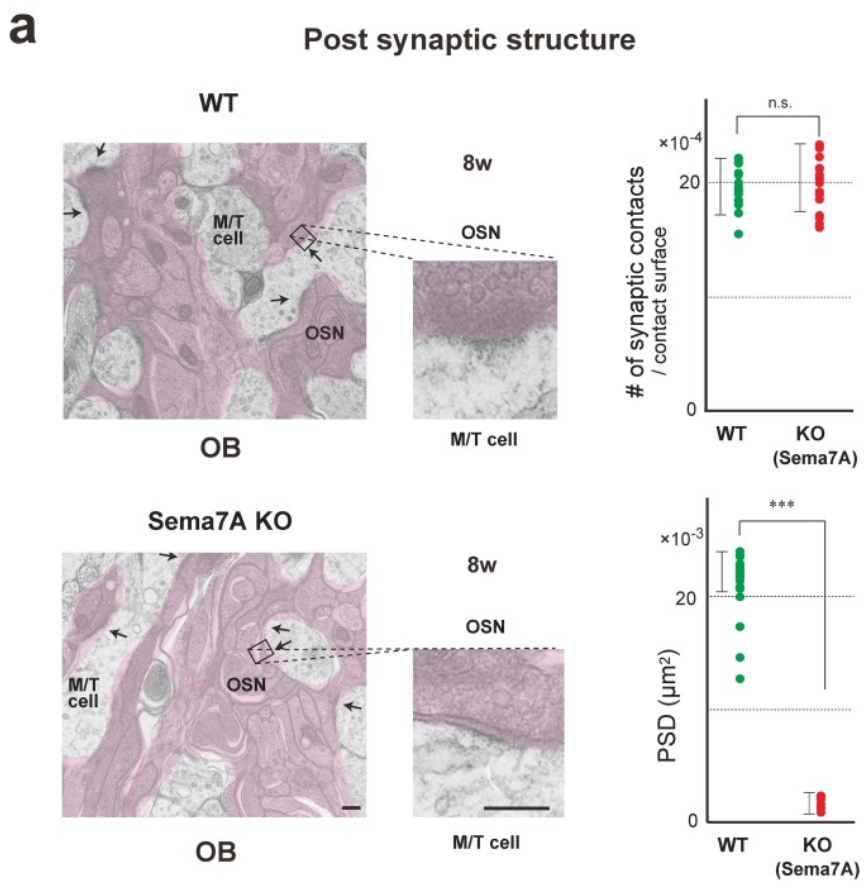
a
Post synaptic structure
WT
8w
M/T cell
OSN
OSN
OB
M/T cell
n.s.
×10-4
20
0
# of synaptic contacts / contact surface
WT
KO (Sema7A)
Sema7A KO
8w
OSN
M/T cell
OSN
OB
M/T cell
***
×10-3
20
0
PSD (μm2)
WT
KO (Sema7A)

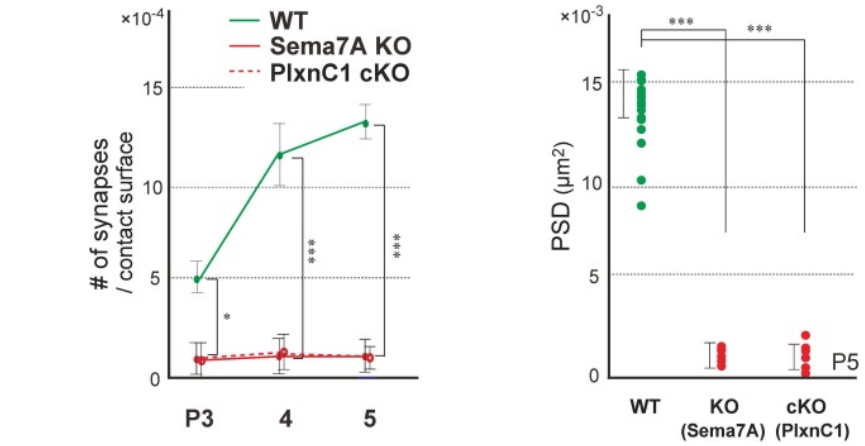
b
Synapse formation
×10-4
WT
Sema7A KO
PlxnC1 cKO
15
10
5
0
# of synapses / contact surface
*
***
***
P3
4
5
×10-3
***
***
15
10
5
0
PSD (μm2)
P5
WT
KO (Sema7A)
cKO (PlxnC1)

Fig. 8 Synapse analysis by EM in the KOs of Sema7A/PlxnC1 signaling.

a, Electron microscopy (EM) analysis of post-synaptic structures. Synaptic contacts and post-synaptic structures were analyzed in the 8w WT, and Sema7A total KO by EM. Arrows indicate synaptic connections. Enlarged views demonstrate that only the surface attachment is formed, but PSD is not matured in the KO. ***p<0.005 (Student's *t*-test). n.s., not significant. Error bars indicate SD (n=3, 4 animals). Scale bars, 300 nm. **b**, The numbers of synaptic structures are compared among the WT, Sema7A total KO, and PlxnC1 cKO in neonates by electron microscopy (left). *p<0.05, ***p<0.005 (Student's *t*-test). Error bars indicate SD (n=2, 2, 5 animals for each line). The area of PSD at P5 are also compared (right). ***p<0.005 (Student's *t*-test). Error bars indicate SD (n=6, 5, 6 animals).

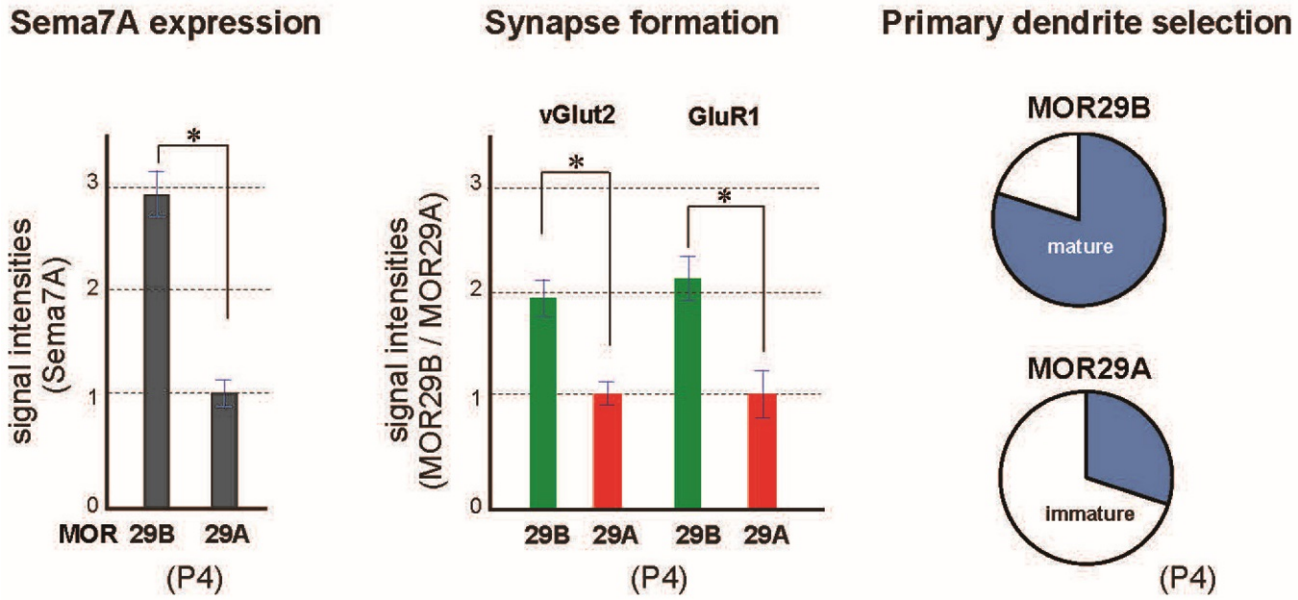

Fig. 9 Sema7A promotes synapse formation and dendrite maturation.

Left, Sema7A expression in the MOR29B and MOR29A glomeruli. OB sections at P4 were immunostained with anti-Sema7A antibodies, and signal intensities of Sema7A are compared between the MOR29B and MOR29A glomeruli. *p<0.05 (Student's *t*-test). Error bars indicate standard deviation SD (n=8 glomeruli). Middle, Synapse formation in the MOR29A and MOR29B glomeruli. OB sections at P4 were also immunostained with antibodies against vGlut2 and GluR1, respectively. Relative fluorescent signals (MOR29B/MOR29A glomeruli) are shown. *p<0.05 (Student's *t*-test). Error bars indicate standard deviation SD (n=8 glomeruli). Right, Primary dendrite maturation of M/T cells in the MOR29A and MOR29B glomeruli. M/T-cell dendrites from single cell were visualized by LY injection into the MOR29A and MOR29B glomeruli at P4. The ratios (%) of mature and immature M/T cells are shown: MOR29A, 8/29 (27.6 %); MOR29B, 22/28 (78.6%). n= 16 glomeruli.

Chapter 4 Sema7A-PlxnC1 interaction for post-synaptic events

In addition to analyses with KOs, we also studied how the Sema7A-PlxnC1 interaction induces synapse formation *in vitro*, using the heterologous system. PSD formation is known to be the earliest event of post-synaptic formation in M/T-cell dendrites[51, 52]. To analyze the role of Sema7A-PlxnC1 interaction in the aggregation of PSD, I introduced the secrete-type of *Sema7A*, *myc*-tagged *PlxnC1* genes and the *FLAG*-tagged gene for SAP90 that serves as a scaffold molecule[53] into HEK293 cells in culture (Fig. 10a). In this system, the secreted Sema7A can interact with PlxnC1 expressed on the HEK-cell surface (Fig. 10b). Staining signals of FLAG-SAP90 was found to be co-localized with those of myc-PlxnC1, when the WT PlxnC1 was interacted with Sema7A in HEK cells (Fig. 10b and c). According to the 3D-structural analyses[54], we introduced amino acid substitution, Y→S at residue 213, into the interaction site of Sema7A with PlxnC1. Then, co-localization of SAP90 with PlxnC1 was blocked with the Y213S mutant Sema7A (Fig. 10b and c). Also, Co-localization was not seen when the cytosolic domain-deleted PlxnC1 (ΔC PlxnC1) was used (Fig. 10b and c). Binding of Sema7A to the cell surface was confirmed by immunostaining with antibodies against Sema7A (Fig. 10b). These data indicate that Sema7A-PlxnC1 interaction leads to recruitment of SAP90 to initiate the post-synaptic events in M/T cells.

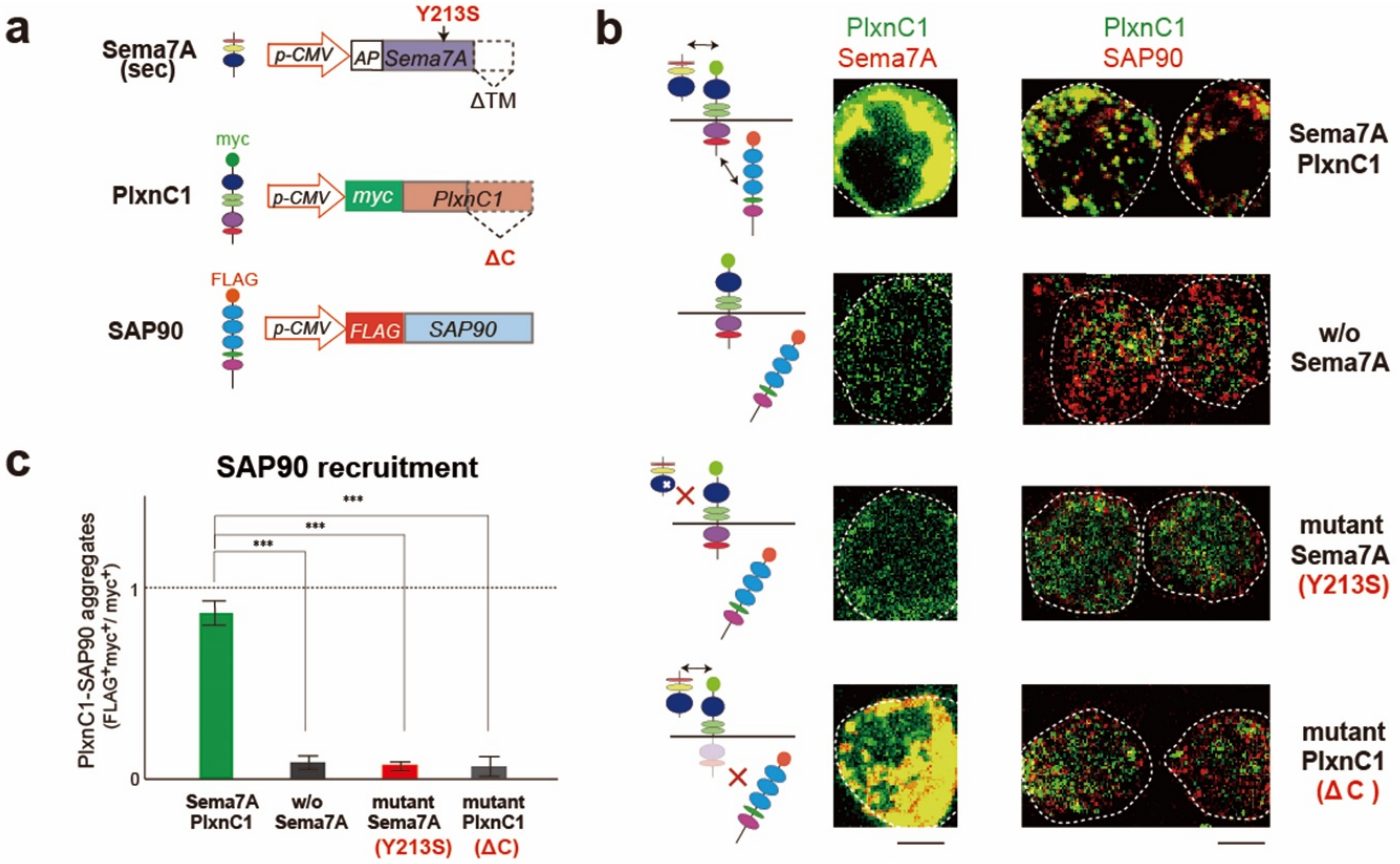
a
Sema7A (sec)
p-CMV
AP
Sema7A
Y213S
ΔTM
PlxnC1
myc
p-CMV
myc
PlxnC1
ΔC
SAP90
FLAG
p-CMV
FLAG
SAP90
b
PlxnC1
Sema7A
PlxnC1
SAP90
Sema7A
PlxnC1
w/o
Sema7A
mutant
Sema7A
(Y213S)
mutant
PlxnC1
(ΔC)
c
SAP90 recruitment
PlxnC1-SAP90 aggregates
(FLAG+myc+/ myc+)
***
***
***
1
0
Sema7A
PlxnC1
w/o
Sema7A
mutant
Sema7A
(Y213S)
mutant
PlxnC1
(ΔC)

Fig. 10 Reconstitution of Sema7A-PlxnC1 interaction *in vitro* culture system.

a, Vector constructs. Schematic diagrams of plasmid structures are illustrated for the secreted form of *Sema7A*, *myc*-tagged *PlxnC1* and *FLAG*-tagged *SAP90*. Y213S mutation in Sema7A and ΔC deletion in PlxnC1 are indicated in the diagrams. **b**, Co-transfection of Sema7A, PlxnC1 and SAP90 in HEK cells. Secrete-form *Sema7A*, *myc*-tagged *PlxnC1* and *FLAG*-tagged *SAP90* genes were introduced into the HEK293 cells in culture system. Structures of Sema7A, PlxnC1, and SAP90 are schematically drawn (left). Cell-surface expression of Sema7A and PlxnC1 was separately analyzed by immunostaining with anti-Sema7A and myc antibodies (middle). In order to detect SAP90 and PlxnC1, cells were immunostained with antibodies against epitope tags FLAG and myc, respectively (right). When Sema7A was co-expressed, aggregation of SAP90 and PlxnC1 was induced. By using mutant Sema7A, Y213S, and the mutant PlxnC1, ΔC blocked PSD formation. Dotted circles show HEK cell. Scale bars, 10μm. **c**, Formation of SAP90 co-localization with PlxnC1. Yellow (red plus green)-stained aggregate-signals (PlxnC1 bound SAP90) are compared among the four different experiments, 1-4, shown in **b**. Aggregation was calculated as $myc^{+}FLAG^{+}$ dots (yellow) / all myc^{+} dots (green and yellow). ***$p<0.005$ (Student's *t*-test). Error bars indicate SD (n=3 trials).

Chapter 5 Signaling pathways downstream of Sema7A-PlxnC1 interaction in M/T cells

What signaling pathway works downstream of Sema7A/PlxnC1 signaling? Little is known about the signaling in the nervous system. Small GTPases are known to play key roles in Plxn-mediated signaling and synaptic functions[55]. Since the Plxn family has the similar cytosolic domain, I focused on both Rac1/Cdc42 and Ras pathways, known to work downstream of PlxnA or PlxnB signaling[55] and promote synapse formation[56]. Based on that Rac1/Cdc42 and Ras signals phosphorylate PAK and ERK[55], respectively, I analyzed rI7 glomeruli for PAK and ERK phosphorylation in the Sema7A KO and PlxnC1 cKO at P3, early stage for synapse formation in rI7 glomeruli. Immunostaining revealed that phosphorylation of PAK, but not ERK, was reduced in the KOs (Fig. 11a). The amount of proteins, as well as the transcripts of PAK and ERK, was not changed in the KOs. I then introduced the transgenic (Tg) *Sema7A* gene with the activity-independent *MOR23* promoter[21] into the Sema7A KO background for constitutive expression of Sema7A. Interestingly, introduced Sema7A, but not the Y213S mutant, rescued the phosphorylation of PAK, but not of ERK, in the Sema7A KO background (Fig. 11b). These results suggest that Sema7A-PlxnC1 interaction activates the Rac1/Cdc42 pathway, but not the Ras, to induce post-synaptic events for synapse formation (Fig. 11d). As mentioned above, not only synapse formation but also dendrite selection is perturbed in the Sema7A KO and PlxnC1 cKO. It may mean that synaptic activity is needed for dendrite selection and branch pruning. We postulate that synaptogenesis triggered by Sema7A-PlxnC1 signaling induces an increase in calcium concentrations, synaptic-activity, in M/T-cell dendrites. To examine "synapto-tropic model" in the OB, I used a NMDA inhibitor, MK801, to pharmacologically block Ca^{2+} entry into M/T cells[57] (Fig. 11c). This treatment blocks synaptic activity after formation of synapses. When transcription levels of *cpg15*, a marker gene for synaptic activity[58], in M/T cells with or without MK801 treatment, MK801 treatment markedly reduced *cpg15* expression (Fig. 11c left). In the rI7 glomeruli, dendrite selection was suppressed by MK801 (Fig. 11c right). These results indicate that synaptic transmission triggers primary dendrite selection in M/T cells by synaptic competition after synapse formation by Sema7A/PlxnC1 signaling (Fig. 11d).

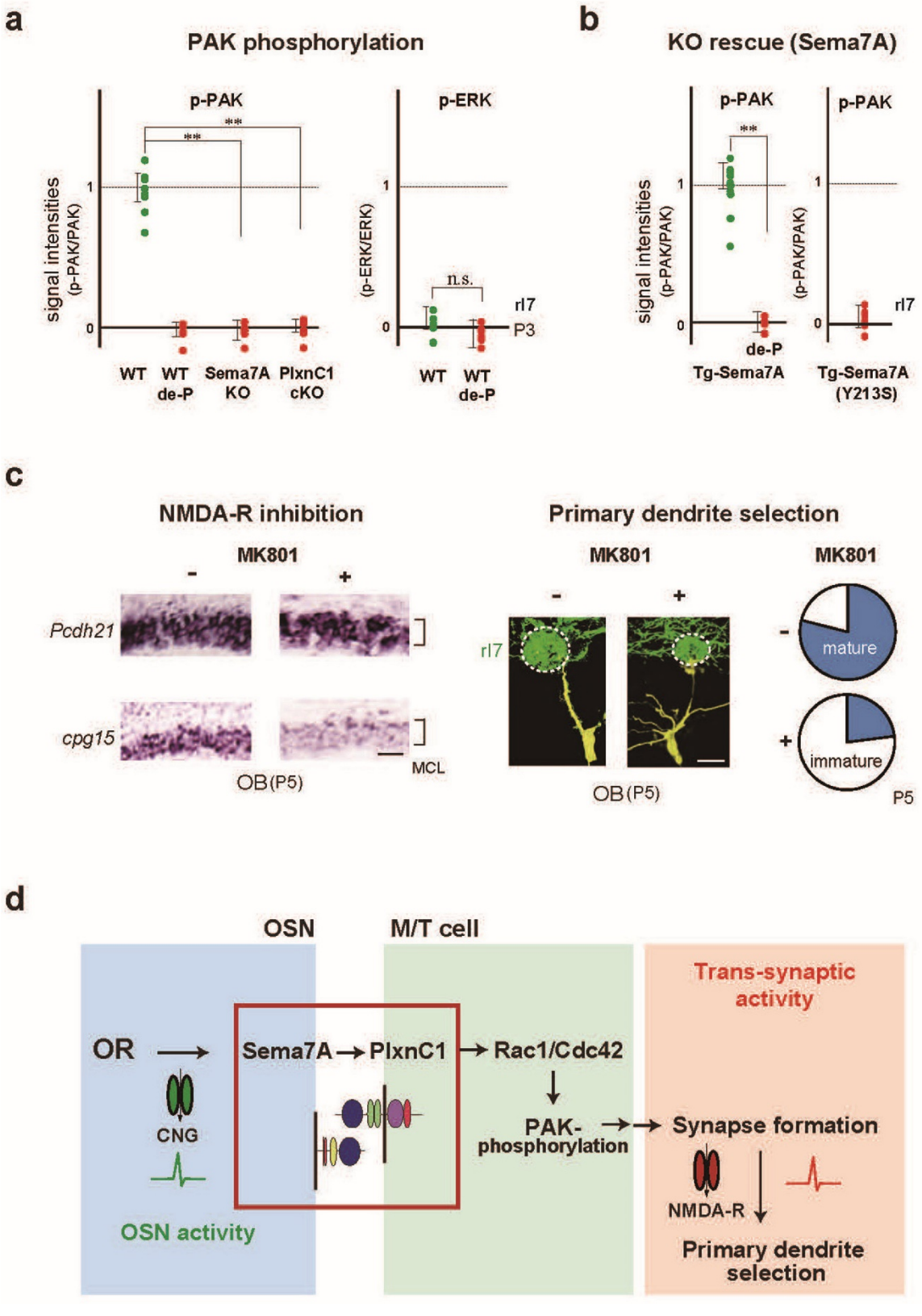
a
PAK phosphorylation
p-PAK
p-ERK
signal intensities
(p-PAK/PAK)
(p-ERK/ERK)
1
0
**
**
n.s.
rl7
P3
WT
WT de-P
Sema7A KO
PlxnC1 cKO
b
KO rescue (Sema7A)
p-PAK
p-PAK
Tg-Sema7A
Tg-Sema7A (Y213S)
c
NMDA-R inhibition
MK801
-
+
Pcdh21
cpg15
MCL
OB(P5)
Primary dendrite selection
MK801
MK801
rl7
mature
immature
P5
d
OSN
M/T cell
Trans-synaptic activity
OR
CNG
Sema7A → PlxnC1
Rac1/Cdc42
PAK-phosphorylation
Synapse formation
NMDA-R
OSN activity
Primary dendrite selection

Fig. 11 Effects downstream of Sema7A/PlxnC1 signaling.

a, Signaling cascades downstream of Sema7A-PlxnCl interaction. Left, Phosphorylation of PAK and ERK in the Sema7A KO and PlxnCl cKO in early neonates. OB sections at P3 were immunostained with antibodies against phosphorylated (p-), and non-phosphorylated forms of PAK and ERK. Phosphatase-treated samples (de-P) were also analyzed as negative controls. Relative fluorescent intensities, p-PAK/PAK and p-ERK/ERK, are compared within the rI7 glomeruli. **p<0.01 (Student's *t*-test). Error bars indicate SD (n=7, 3, 4, 5 glomeruli for WT, de-P, Sema7A KO, and PlxnC1 cKO). **b**, Rescue of PAK- phosphorylation in the Sema7A KO by introducing the Tg *Sema7A* gene. This recovery is blocked by the Sema7A mutation, Y213S, which interferes with PlxnC1 interaction. By crossing the transgenic animal, the WT or mutant *Sema7A* gene was introduced into the Sema7A KO mice, and was expressed constitutively in the rI7-expressing OSNs. OB sections at P3 were immunostained with antibodies against p-, and non-p forms of PAK. De-P samples were also analyzed. Relative fluorescent intensities p-PAK/PAK within the rI7 glomeruli are compared between the WT and mutant Sema7A. **p<0.01 (Student's *t*-test). Error bars indicate SD (n=3 mice for the WT Sema7A, n=2 mice for the mutant Sema7A). **c**, Pharmacological inhibition of the trans-synaptic activity in M/T cells. Left, Inhibition of the synaptic activity with an NMDA-R inhibitor, MK801. OB sections at P5 were analyzed by *in situ* hybridization for the expression of *Pcdh21* (mitral cell marker) and *cpg15* (synaptic-activity marker). EYFP-tagged rI7 glomeruli were identified by GFP-staining. The expression of *cpg15* in M/T cells was inhibited after MK801 injection. n=3 animals. Scale bar, 20μm. Right, Dendrite maturation of the MK801-treated M/T cells at P5. M/T cells were visualized by LY injection into the rI7 glomeruli. The ratios (%) of mature (blue) and immature M/T cells are shown: $MK801^{-}$, 19/25 (76.0 %); $MK801^{+}$, 6/25 (24.0 %). n= 19 glomeruli. Scale bar, 10μm. **d**, Schematic diagram of synapse formation regulated downstream of Sema7A signaling. OR-derived-neuronal activity induces Sema7A expression in OSNs, Sema7A interacts with PlxnC1 in M/T-cell dendrites and activates the Cdc42/Rac1-PAK signaling cascade to initiate synapse formation. Activities via synapses are responsible for dendrite selection and maturation. MCL, mitral-cell layer.

Chapter 6-12 were omitted in this version.

Conclusion & Perspectives

In this study, I described functional two types of neuronal activities: one is the OR-derived activity that regulates Sema7A expression in OSN axons and the other is trans-synaptic activity for dendrite selection in M/T cells. In the mouse olfactory system, adapted olfactory circuits can be established by selecting primary dendrites of M/T cells in an activity-dependent manner regulated by Sema7A signaling during the critical period. Then, the imprinted odor memory in the OB newly activates the aMeA for attractive social responses, and suppresses the AmPir known to induce ACTH through oxytocin modulation. Now I declare that the mouse olfactory system will continue serving as an excellent model system for the study of neurodevelopmental disorders, decision making and memory formation mechanism in the mammalian brain.

Future study should clear several questions; 1, wheather the mouse critical period could be changed by artificial modulation of PlxnC1 expression. 2, how and where the oxytocin works to add the attractive quality to the imprinted memory. 3, what mechanisms work for forming the critical period in the other sensory system. 4, how our work contribute to understand of neurodevelopmental disorders, such as ASD and attachment disorders.

Material and Methods

Mice

CNG-A2 KO and Sema7A total KO mice were purchased from The Jackson Laboratory (No: 002905, No: 005128). Both the KO mice for oxytocin[73] and oxytocin receptor[74] were provided by K. Nishimori at Tohoku University. BAC Tg mice containing the *MOR29A* and *MOR29B*[44], Tg mice expressing the *rI7* with the *MOR23* promoter[21], rI7 (RDY)-ires-gap-YFP mice[21], OSN-specific cKO of Nrp1[82], and MOR28-knockin mice[45] were generated previously in my group. In order to generate cell-type-specific Sema7A and PlxnC1 knockout in the Cre driver line, we cloned exon 5 of the *Sema7A* and exon 5 of the *PlxnC1* gene into the double-floxed, inverted open-reading frame plasmid DT-A/Conditional FW (http://www.cdb.riken.jp/arg/cassette.html). The cKOs were generated according to the published protocol (http://www.cdb.riken.jp/arg/tg.html). The Pcdh21-Cre mouse (RBRC02189) was purchased from RIKEN[50]. (http://www.cdb.riken.jp/arg/tg.html). All animal experiments were approved by the Animal Care Committee in the University of Fukui, Tokyo University and RIKEN institute in Kobe.

Antibodies

Antibodies against Sema7A (goat, 1:3000, #AF-1835), PlxnC1 (goat, 1:3000, discontinued), and CNG-A2 (rabbit, 1:200, #APC-045), vGlut2 (guinea pig, 1:1000, #AB2251-l), GluR1 (rabbit, 1:1000, #ab51092), GFP (rabbit, 1:1000, #A-10260), Lucifer yellow (rabbit, 1:2000, #A-5750), and OMP (goat, 1:2000, #Cat. No. 019-22291), were purchased from R&D Systems, Abcam, Alomone Labs, Millipore, Invitrogen, Abcam, Thermo Fisher Scientific, Thermo Fisher Scientific, and Wako Chemicals, respectively. Antibodies against PAK, p-PAK, ERK, and p-ERK (rabbit, 1:1000, #2602, #2606, #4372, #4370) were obtained from Cell Signaling. Antibodies against FLAG (rabbit, 1:1000, #ab2492), c-myc (mouse, 1:1000, #ab32) and EGR1 (rabbit, 1:1000, #ab6054) were from Abcam.

In Situ Hybridization

In order to prepare cRNA probes, DNA fragments of 500-3000 bp were amplified by PCR from the OB cDNA of C57BL/6 mice. Unique sequences for each gene were amplified. PCR products were subcloned into pGEM-T vector (Promega) as templates to make cRNA probes. Hybridization was performed according to the standard method[22]. Primer sequences used are as follows: *sema7A*, 5'-gctccattgcagaaggtttc-3' (forward) and 5'-gctcacagctctgttccaca-3' (reverse); *plxnC1,* 5'-gggactttcaagcgactgag-3' (forward) and 5'-agtgtcttgcggagatgctt-3' (reverse); *integrinβ1,* 5'-gaaggtggctttgatgcaat-3' (forward) and 5'-tgttggaacactttcgtcca-3' (reverse).

Immunostaining

For immunohistochemistry, OB sections were perfused with 4% paraformaldehyde (PFA) in PBS and treated with the primary and secondary antibodies[22]. These sections were photographed with a fluorescence microscope, Model IX70 (Olympus), coupled to a cooled CCD camera, C4742-95-12ERG (Hamamatsu Photonics).

Immunoelectron Microscopy

Mice were transcardially perfused with 4% PFA and 0.1% glutaraldehyde (GA) in 0.1 M phosphate buffer (PB), immersed in the same buffer at 4°C for 1-2 hr, and then sectioned transversely into 50-μm slices with a vibratome, LinearSlicer PRO7 (D.S.K.). The sections were rinsed in 0.1 M PB, incubated in 0.1 M PB with 2% normal serum for 1 hr, and then incubated within primary antibody in 1% normal serum over-night at 4°C. Then sections were rinsed in 0.1 M PB, incubated with Vector Labs biotinylated secondary immunoglobulin for 60 min, rinsed in 0.1 M PB, incubated in the Molecular Probes Nanogold for 90 min, and again rinsed in 0.1 M PB. The samples were incubated in 0.1% GA for 10 min, and in Molecular Probes Silver Enhance Kit for 3-5 min. The protocol for electron microscopy was described in the next section.

Electron microscopy

Mice were transcardially perfused with 2% PFA and 2.5% GA in 0.1 M PB. The mice were then immersed in the same buffer at 4°C for 1-2 hr and rinsed in 0.1 M PB before being sectioned

transversely into 50-μm slices with a vibratome. The sections were incubated in 2% osmium tetroxide for 60 min, dehydrated through an ascending ethanol series, and embedded in EPON. Sections (70-100 nm) were then sliced with EM UC7 (Leica), mounted on Cu grids, and examined in a transmission electron microscope VE-9800 (KEYENCE). Images were taken at primary magnification.

Naris Occlusion

Unilateral naris occlusion was performed at P0 on the right nostril with an electrical cautery, SURE SX-10C (Ishizaki, Japan), and the occluded pups were daily examined to ensure the blockade of occluded nostril by checking the scar formation. The right-side naris was reopened at various time points during the postnatal period using a 31G needle or, at the end of closing, mice were sacrificed for analysis by immunohistochemistry.

Intracellular Injection

Intracellular injection[49] was performed as below. Under a water-immersion 40× objective lens, a micropipette was inserted into a GFP-labelled glomerulus. After labeling, slices were thinned and incubated with a blocking solution containing 5% serum and 0.5% Triton-X in PBS. Samples were incubated with rabbit polyclonal anti-LY antibodies and chicken anti-GFP antibodies, then incubated with Alexa Fluor 488-conjugated goat anti-rabbit IgG (H+L) conjugate and Alexa Fluor 555-conjugated goat anti-chicken IgG (H+L) (Thermo Fisher Scientific, 1:200 dilution).

Alkaline-Phosphatase (AP) Binding Assay

To generate fusion proteins, cDNAs of the ectodomain were introduced into the APtag-5 (GenHunter Corporation) of AP fusion vectors. DNA fragments of the ectodomain were obtained by PCR to fuse the N terminus of AP. AP fusion proteins were generated in the transfected HEK293T cells and concentrated using Centriprep (Millipore). Frozen OB sections were postfixed at −20°C for 20 min in 100% methanol. AP staining was performed as the standard method[20, 22, 43].

In Vitro Binding Assay

Coding sequences of mouse SAP90, PlxnC1, and ectodomain of Sema7A were cloned into pCMV-SC-NF (STRATAGENE), pCMV-SC-NM (STRATAGENE), and APtag-5 (GenHunter Corporation), respectively. FLAG-tag was attached to the N-terminal of SAP90. Myc-tag was introduced between the signal peptide and semaphorin domain of PlxnC1. The Y213S mutant of Sema7A was generated by PCR on the *Sema7A* cDNA (pCMV-AP-secret type Sema7A mut)[54]. The cytosolic domain in the *PlxnC1* gene was deleted by PCR to generate pCMV-c-myc-ΔC PlxnC1. Co-transfection of HEK293 cells was performed as described previously [20, 22, 43]. Two days after transfection, HEK cells were attached, fixed on micro slides and processed for immunocytochemistry with antibodies against FLAG, myc, and Sema7A.

Drug Administration

MK-801 (Sigma–Aldrich) dissolved in normal saline to achieve a final concentration of 0.02 mg/kg or saline injected into the dorsal OB, with a stainless steel needle (30 gauges), twice a day from P2 to P5 in two groups of littermates.

Intensity Measurement

For fluorescent signals of immunostaining, digital pictures were captured with a digital CCD camera, C4742-95-12ERG (Hamamatsu Photonics), and two-photon microscopy (Olympus). Tone was reversed and a monochrome picture was used for the measurement. For OB sections, digital images were captured with a digital CCD camera, Model DP70 (Olympus). For quantitation of the staining level of each glomerulus, the mean pixel intensity within the region surrounded by the periglomerular cell nuclei was measured using Scion Image (Scion Corp.).

Neonatal Odor Conditioning

Before conditioning, mother mice were pre-exposed to the odor for 10 min, three times a day for 3 consecutive days. A filter paper (2x2 cm) spotted with a test odor was placed near the mice. For conditioning, pups were exposed to the odor for 10 min with the foster mother, three times a day for

3 consecutive days. Odor concentrations used here were 0.5μl of 20 mM for VNL, 100 mM for 4MT, 100 mM for PPA, and 100 mM for BUT.

Habituation/Dishabituation Test

For the test, adult littermates (6w-old male) were kept individually in a new cage (26x40x18 cm) containing a plain filter paper for 5 min before the experiment. This treatment was to habituate the mice to a filter paper and to evaluate the net curiosity to a test odor in the following filter presentation. During the test, about 8% of total mice did not demonstrate any interest in the plain filter paper, which were precluded. In the test, a filter paper with 0.5μl of distilled water was intermittently presented for 3 min. This was repeated three times with 1-min intervals. Next, a filter paper spotted with the 1st test odorant was presented three times (habituation). Then, the 2nd test odorant was also presented three times (dishabituation). Investigation times (sec) during each odorant presentation were measured. In this test, the mice were used only once avoiding to confound the data due to the previous learning. The test was blindly performed to avoid unconcious bias and to insure the objectivity. The mouse behavior was taken with a digital video camera, DCR-SR100 (SONY). Investigation was defined as a nasal contact with filter papers within 1 mm of distance. Odors used were vanillin (Wako), eugenol (Tokyo-Kasei), (–)-carvone (Sigma-Aldrich), (+)-carvone (Sigma-Aldrich), and 4-methyl thiazole (Wako).

Odor Preference Test

For the preference test[59], adult littermates (6w male) were individually habituated in the cage (26x40x18 cm) with clean beds. A filter paper (2x2 cm) with 0.5μl of odor sample and another filter paper with 0.5μl of distilled water were carefully placed not to disturb the mice in the diagonal corners. Times (sec) in the room with or without a test odorant during the 5-min test period were measured. The positions of filter papers were alternated, avoiding side preference. The mice were used only once to avoid bias attribute to learning. The mouse behaviour was taken with a digital video camera, DCR-SR100 (SONY). The videos were randomized and scored blindly. Odors used were propionic acid (Tokyo-Kasei), vanillin (Wako), 4-methyl thiazole (Wako), food pellet (SLC), and butyric acid (TGI).

Stress-Induced Hyperthermia Test

For the stress-induced hyperthermia test[60], mice (6w) were individually habituated to the cage and checked their body temperature before the test. The mice were then transferred to a new cage and exposed to a test odor. The rectal temperature was measured by using a digital thermistor, BAT-12 (Physitemp Instruments Inc.), which probe was inserted to a length of 10-20 mm intrarectal until stable reading was obtained. Temperature differences before (T) and after (Tx) the transfer were individually measured every 5 min.

Social Behavioral Responses

For the social response test, 6w littermates were individually habituated in a new cage (26x40x18 cm). The test was followed as described by Silverman et al. (2010)[83]. The clean beds and beds with unfamiliar mouse scent were carefully placed not to disturb the mice in the opposite diagonal corners of the test cage. Avoiding direct contacts of the mouse nose, the bed samples were presented in a small plastic cup. The positions of cups were alternated to avoid side preference. This apparatus evaluates a simple olfactory social interest in the volatile smell of unfamiliar mice, excluding visual, auditory, and vomeronasal inputs. Times (sec) in the room with or without unfamiliar mouse odor were measured during the 5-min test period. The mice were used only once avoiding confoundation of the data due to learning. The test was blindly performed to avoid unconcious bias to insure the objectivity. The mouse behavior was taken with a digital video camera, DCR-SR100 (SONY).

Three-Chamber Social Interaction Test

6w littermate mice were used in the experiment. The three-chamber test was followed as described by Moy et al. (2004)[63]. Before the test, the mouse was allowed to explore all three chambers divided with plastic walls for 10 min. The test mouse was placed in the center chamber, an empty plastic cage was to the right, and an unfamiliar mouse (male C57BL6) in a cage was to the left. The test mouse was allowed to move freely for 15 min. The mouse behavior was taken with a digital

video camera, DCR-SR100 (SONY). Time duration in each room was measured during the 15-min test period. The positions of the empty cage and unfamiliar mouse were alternated to avoid side preference.

ACTH Assay

For the ACTH measurement[28], mice were housed individually to minimize the background level of plasma ACTH. After exposing to a test odorant for 10 min, the mice were decapitated quickly and blood samples were collected. Plasma ACTH concentrations were measured by using the ACTH ELISA kit (MD Biosciences).

Intranasal Administration of Oxytocin

Oxytocin (40 IU/ml) (Syntocinon, Defiante Faramceutica S.A.) in 1M PBS or PBS alone was administered bilaterally in the rhinal cavities of neonates. Oxytocin (0.15 IU in 5μl) was given three times a day from P1 to P6 according to the procedure described by Galbusera et al. (2017)[75]. The test was done with a group of 4~6 mice for each experiment. The solution was applied with a P20 pipette. The administrated mouse was held with its nose up to ensure that liquid was inhaled and diffused into nostrils thoroughly. Both nostrils were treated with oxytocin, one by one. The mouse was then reposited to its home cage with its littermates until the test was done. For the administration of adult mice, 0.15 IU oxytocin in 20μl of PBS was intranasally administrated acutely before the odor preference test.

Statistical Analyses

All statistical analyses were performed by using Excel 2003 (Microsoft) with the Statcel2 add-on (OMS).

References

1. Hong, W. & Luo, L. Genetic control of wiring specificity in the fly olfactory system. *Genetics* **196**, 17-29 (2014).
2. Luo, L., Callaway, E. M. & Svoboda, K. Genetic dissection of neural circuits. *Neuron* **57**, 634-660 (2008).
3. Yogev, S. & Shen, K. Cellular and molecular mechanisms of synaptic specificity. *Annu. Rev. Cell Dev. Biol.* **30**, 417-437 (2014).
4. Espinosa, J. S. & Stryker, M. P. Development and plasticity of the primary visual cortex. *Neuron* **75**, 230-249 (2012).
5. Hensch, T. K. Critical period plasticity in local cortical circuits. *Nat. Rev. Neurosci*. **6**, 877-888 (2005).
6. Hooks, B. M. & Chen, C. Critical periods in the visual system: changing views for a model of experience-dependent plasticity. *Neuron* **56**, 312-326 (2007).
7. Kirkby, L. A., Sack, G. S., Firl, A. & Feller, M. B. A role for correlated spontaneous activity in the assembly of neural circuits. *Neuron* **80**, 1129-1144 (2013).
8. Okawa, H., Hoon, M., Yoshimatsu, T. L., Santina, D. & Wong, R. O. Illuminating the Multifaceted Roles of Neurotransmission in Shaping Neuronal Circuitry. *Neuron* **83**, 1303-1318 (2014).
9. Costanzo, R. M. Regeneration of olfactory receptor cells. *Ciba. Found. Symp.* **160**, 233-248 (1991).
10. Graziadei, P. P. & Monti Graziadei, G. A. Neurogenesis and plasticity of the olfactory sensory neurons. *Ann. Y. Acad. Sci.* **457**, 127-142 (1985).
11. Leung, C. T., Coulombe, P. A. & Reed, R. R. Contribution of olfactory neural stem cells to tissue maintenance and regeneration. *Nat. Neurosci.* **10**, 720-726 (2007).
12. Ma, L. et al. A developmental switch of axon targeting in the continuously regenerating mouse olfactory system. *Science* **344**, 194-197 (2014).
13. Tsai, L. & Barnea, G. A critical period defined by axon-targeting mechanisms in the murine olfactory bulb. *Science* **344**, 197-200 (2014).
14. Buck, L. B., & Axel, R. A novel multigene family may encode odorant receptors: a molecular basis for odor recognition, *Cell* **65**, 175-187 (1991).
15. Rodriguez, I. Singular expression of olfactory receptor genes, *Cell* **155**, 274-277 (2013)

16. Mombaerts, P. et al. Visualizing an olfactory sensory map, *Cell* **87,** 675-686 (1996).
17. Malnic, B., Hirono, J., Sato,T., & Buck, L. B. Combinatorial receptor codes for odors, *Cell* **96**, 713-723 (1999).
18. Mori, K. & Sakano, H. How is the olfactory map formed and interpreted in the mammalian brain, *Annu. Rev. Neurosci.* **34**, 467-499 (2011).
19. Neville, K. R. & Haberly, L. B. Olfactory cortex. In: The synaptic organization of the brain, *New York: Oxford UP*. Ed **5** (Shepherd GM, edited), 415-454 (2004).
20. Takeuchi, H. et al. Sequential Arrival and Graded Secretion of Sema3F by Olfactory Neuron Axons Specify Map Topography at the Bulb, *Cell* **141**, 1056-1067 (2010).
21. Imai, T., Suzuki, M. & Sakano, H. Odorant receptor-derived cAMP signals direct axonal targeting, *Science* **314**, 657-661 (2006).
22. Serizawa, S. et al. A neuronal identity code for the odorant receptor-specific and activity-dependent axon sorting, *Cell* **127**, 1057-1069 (2006).
23. Kermen, F. et al. Topographical representation of odor hedonics in the olfactory bulb. *Nat. Neurosci.* **19**, 876–878 (2016).
24. Mori, K. & Sakano, H. How is the olfactory map formed and interpreted in the mammalian brain? *Ann. Rev. Neurosci.* **34**, 467-499 (2011).
25. Inokuchi, K. et al. *Nrp2* is sufficient to instruct circuit formation of mitral-cells to mediate odor-induced attractive social responses. *Nat. Commun.* **8**, 15977 (2017).
26. Lehman, M. N., Winans, S. S. & Powers, J. B. Medial nucleus of the amygdala mediates chemosensory control of male hamster sexual behavior. *Science* **210**, 557–560 (1980).
27. Maras, P. M. & Petrulis, A. Chemosensory and steroid-responsive regions of the medial amygdala regulate distinct aspects of opposite-sex odor preference in male Syrian hamsters. *Eur. J. Neurosci.* **24**, 3541–3552 (2006).
28. Day, H. E., Masini, C. V. & Campeau, S. The pattern of brain *c-fos* mRNA induced by a component of fox odor; 2,5-dihydro-2,4,5-trimethylthiazoline (TMT), in rats, suggests both systemic and processive stress characteristics. *Brain Res.* **1025**, 139–151 (2004).
29. Miyamichi, K. et al. Cortical representations of olfactory input by trans-synaptic tracing. *Nature* **472**, 191-196 (2011).
30. Root, C. M., Denny, C.A. Hen, R. & Axel, R. The participation of cortical amygdala in innate, odour-driven behaviour. *Nature* **515**, 269-273 (2014).
31. Logan, D. W. et al. Learned recognition of maternal signature odors mediates the first suckling

episode in mice. *Curr. Biol.* **22**, 1998-2007 (2012).

32. Mennella, J. A., Jagnow, C. P. & Beauchamp, G. K. Prenatal and postnatal flavor learning by human infants. *Pediatrics* **107**, 6:e88 (2001).
33. Sullivan, R. M., Landers, M., Yeaman, B. & Wilson, D. A. Good memories of bad events in infancy. *Nature* **407**, 38-39 (2000).
34. Wilson, D. A. & Sullivan, R. M. Neurobiology of associative learning in the neonate: Early olfactory learning. *Behav. Neural Biol.* **61**, 1-18 (1994).
35. Nevitt, G. A., Dittman, A. H., Quinn, T. P. & Jr. Moody, W. J. Evidence for a peripheral olfactory memory in imprinted salmon. *Proc. Natl. Acad. Sci. U.S.A.* **91**, 4288-4292 (1994).
36. Horn, G. Visual imprinting and the neural mechanism of recognition memory. *Trends Neurosci.* **7**, 300-305 (1998).
37. Nakamori, T., Maekawa, F., Sato, K., Tanaka, K. & Ohki-Hamazaki, H. Neural basis of imprinting behavior in chicks. *Dev. Growth Differ.* **55**, 198-206 (2013).
38. Lin, D. M. et al. Formation of precise connections in the olfactory bulb occurs in the absence of odorant-evoked neuronal activity, *Neuron* **26**, 69-80 (2000).
39. Zhao, H. & Reed, R. R. X inactivation of the OCNC1 channel gene revealed a role for activity-dependent competition in the olfactory system, *Cell* **104**, 651-660 (2001).
40. Pasterkamp, R. J., Peschon, J. J., Spriggs, M. K. & Kolodkin, A. L. Semaphorin 7A promotes axon outgrowth through integrins and MAPKs. *Nature* **424**, 398-405 (2003).
41. Tamagnone, L. et al. Plexins are a large family of receptors for transmembrane, secreted, and GPI-anchored semaphorins in vertebrates. *Cell* **99**, 71-80 (1999).
42. Suzuki, K. et al. Semaphorin 7A initiates T-cell-mediated inflammatory responses through alpha1beta1 integrin, *Nature* **446**, 680-684 (2007).
43. Flanagan, J. G. & Cheng, H. J. Alkaline phosphatase fusions of ligands or receptors as in situ probes for staining of cells, tissues, and embryos, *Methods Enzymol.* **327,** 19-35 (2000).
44. Tsuboi, A. et al. Two highly homologous mouse odorant receptors encoded by tandemly linked MOR29A and MOR29B genes differently respond to phenyl ethers. *Eur. J. Neurosci.* **33**, 205-213 (2011).
45. Serizawa, S. et al. Mutually exclusive expression of odorant receptor transgenes, *Nat. Neurosci.* **3**, 687-693 (2000).
46. Kasowski, H. J., Kim, H. & Greer, C. A. Compartmental organization of the olfactory bulb glomerulus, *J. Comp. Neurol.* **407**, 261-274 (1999).

47. Honma, S., Kawano, M., Hayashi, S., Kawano, H. & Hisano, S. Expression and immunohistochemical localization of vesicular glutamate transporter 2 in the migratory pathway from the rat olfactory placode. *Eur. J. Neurosci*.**4**, 923-936 (2004).
48. Montague, A. A. & Greer, C. A . Differential distribution of ionotropic glutamate receptor subunits in the rat olfactory bulb. *J. Comp. Neurol.* **405**, 233-246 (1999).
49. Naritsuka, H., Sakai, K., Hashikawa, T., Mori, K. & Yamaguchi, M. Perisomatic-targeting granule cells in the mouse olfactory bulb, *J. Comp. Neurol.* **515**, 409-426 (2009).
50. Nagai, Y., Sano, H. & Yokoi, M. Transgenic expression of Cre recombinase in mitral/tufted cells of the olfactory bulb. *Genesis* **43**, 12-16 (2005).
51. SY. Chen, HJ. Cheng, Functions of axon guidance molecules in synapse formation, *Curr. Opin. Neurobiol.* **19**, 471-478 (2009).
52. Siddiqui, T. J. & Craig, A. M. Synaptic organizing complexes, *Curr. Opin. Neurobiol.* **21**, 132-143 (2011).
53. Burkhardt, C. et al. Semaphorin 4B interacts with the post-synaptic density protein PSD-95/SAP90 and is recruited to synapses through a C-terminal PDZ-binding motif, *FEBS Lett.* **579**, 3821-3828 (2005).
54. Liu, H. et al. Structural Basis of Semaphorin-Plexin Recognition and Viral Mimicry from Sema7A and A39R Complexes with PlexinC1, *Cell* **142**, 749-761 (2010).
55. Boda, B., Dubos, A. & Muller, D. Signaling mechanisms regulating synapse formation and function in mental retardation, *Curr. Opin. Neurobiol.* **20**, 519-527 (2010).
56. Negishi, M., Oinuma, I. & Katoh, H. Plexins: axon guidance and signal transduction, *Cell. Mol. Life Sci.* **62**, 1363-1371 (2005).
57. Woodruff, G. N. et al. The interaction between MK-801 and receptors for N-methyl-D-aspartate: functional consequences, *Neuropharmacology* **26**, 903-909 (1987).
58. Nedivi, E., Wu, G. Y. & Cline, H. T. Promotion of dendritic growth by CPG15, an activity-induced signaling molecule, *Science* **281**, 1863-1866 (1998).
59. Saraiva, R. L. et al. Combinatorial effects of odorants on mouse behavior. *Proc. Natl. Acad. Sci. U.S.A.* **113**, 3300-3306 (2016).
60. Spooren, W. P., Schoeffter, P., Gasparini, F., Kuhn. R. & Gentsch, C. Pharmacological and endo crinological characterization of stress-induced hyperthermia in singly house mice using classical and candidate anxiolytics (LY314582, MPEP and NKP608). *Eur. J. Pharmacol.* **435**, 161-170 (2002).

61. Liu, A., Savya, S. & Urban, N. N. Early odorant exposure increases the number of mitral and tufted cells associated a single glomerulus. *J. Neurosci.* **36**, 11646-11653 (2016).
62. Todrank, J., Heth, G. & Restrepo, D. Effects of in utero odorant exposure on neuroanatomical development of the olfactory bulb and odour preferences. *Proc Biol Sci.* **278**, 1949-552011 (2011).
63. Moy, S. S. et al. Sociability and preference for social novelty in five inbred strains: an approach to assess autistic-like behavior in mice. *Genes Brain Behav.* **3**, 287-302 (2004).
64. Kondoh, K. et al. A specific area of olfactory cortex involved in stress hormone responses to predator odors. *Nature* **532**, 103–106 (2016).
65. Anderson, K. E. Neurotransmitters: central and peripheral mechanisms. *Int. J. Impot. Res.* **4**, S26-33 (2000).
66. De Wied, D., Diamant, M. & Fodor, M. Central nervous system effects of the neurohypophyseal hormones and related peptides. *Front. Neuroendocrinol.* **14**, 251-302 (1993).
67. Gur, R., Tendler, A. & Wagner, S. Long-term social recognition memory is mediated by oxytocin-dependent synaptic plasticity in the medial amygdala. *Biol. Phychiatry* **76**, 377-386 (2014).
68. Bosch, O. J. & Young, L. J. Oxytocin and social relationships: From attachment to bond disruption. *Curr. Top Behav. Neurosci.* **35**, 97-117 (2018).
69. Donaldson, Z. R. & Young, L. J. Oxytocin, vasopressin, and the neurogenetics of sociality. *Science* **322**, 900-904 (2008).
70. Insel, T. R. The challenge of translation in social neuroscience: a review of oxytocin, vasopressin, and affiliative behavior. *Neuron* **65**, 768-779 (2010).
71. Muscatelli, F., Desarménien, M. G., Matarazzo, V. & Grinevich, V. Oxytocin signaling in the early life of mammals: link to neurodevelopmental disorders associated with ASD. *Curr. Top Behav. Neurosci.* **35**, 239-268 (2018).
72. Sannino, S., Chini, B. & Grinevich, V. Lifespan oxytocin signaling: Maturation, flexibility, and stability in newborn, adolescent, and aged brain. *Dev. Neurobiol.* **77**, 158–168 (2017).
73. Nishimori, K. et al. Oxytocin is required for nursing but is not essential for parturition or reproductive behavior. *Proc. Natl. Acad. Sci. USA.* **93**, 11699–11704 (1996).
74. Takayanagi, T. et al. Pervasive social deficits, but normal parturition, in oxytocin receptor-deficient mice. *Proc. Natl. Acad. Sci. USA.* **102**, 16096–16101 (2005).

75. Galbusera, A. et al. Intranasal oxytocin and vasopressin modulate divergent brainwide functional substrates. *Neuropsychopharmacology*. **42**, 1420-1434 (2017).
76. Johnson, Z. V. & Young, L. J. Neurobiological mechanisms of social attachment and pair bonding. *Curr. Opin. Behav. Sci.* **3**, 38-44. (2015).
77. Tully, J., Gabay, A. S., Brown, D., Murphy, D. G. M. & Blackwood, N. The effect of intranasal oxytocin on neural response to facial emotions in healthy adults as measured by functional MRI: A systematic review. *Psychiatry Res.* **272**, 17-29 (2018).
78. Missler, M., Südhof, T. C. & Biederer, T. Synaptic Cell Adhesion, *C. S. H. Persp. in Biol*. **4**, 1-18 (2012).
79. Vaughn, J. E., Barber, R. P. & Sims, T. J. Dendritic development and preferential growth into synaptogenic fields: A quantitative study of Golgi-impregnated spinal motor neurons, *Synapse* **2**, 69–78 (1988).
80. Mizrahi, A. & Katz, L. C. Dendritic stability in the adult olfactory bulb, *Nat. Neurosci*. **6**, 1201-1207 (2003).
81. McInnes, L.A. et al. A large-scale survey of the novel 15q24 microdeletion syndrome in autism spectrum disorders identifies an atypical deletion that narrows the critical region. *Mol. Autism* **1**, doi: 10.1186/2040-2392-1-5 (2010).
82. Imai, T. et al. Pre-target axon sorting establishes the neural map topography. Science ***325***, 585-590 (2009).
83. Silverman, J. L., Yang, M., Lord, C. & Crawley, J. N. Behavioural phenotyping assays for mouse models of autism. *Nat. Rev. Neurosci.* **11**, 490-502 (2010).

Acknowledgement

We are grateful to Naritsuka, H. for her advice in single-cell labeling, to Sagara, H. for his help in EM analyses, to Kikusui, T. for his advice in behavioral experiments, to Nishimori, K. for dividing the mutant mice, and to Kiyonari, H. for his help in generating the tg mice. We thank Otsuka, A. J. and members of our laboratory for valuable suggestions and discussion.